PL-TR--95-1123

PL-TR--
95-1123

LIGHTWEIGHT, LIGHT-TRAPPED, THIN GaAs SOLAR CELLS FOR SPACECRAFT APPLICATIONS

Margaret H. Hannon

AstroPower, Inc.
Solar Park
Newark, DE 19716-2000

October 1995

19960305 090

Final Report

Distribution authorized to DoD components only; Proprietary Information; October 1995. Other requests for this document shall be referred to AFMC/STI.

WARNING - This document contains technical data whose export is restricted by the Arms Export Control Act (Title 22, U.S.C., Sec 2751 et seq.) or The Export Administration Act of 1979, as amended (Title 50, U.S.C., App. 2401, et seq.). Violations of these export laws are subject to severe criminal penalties. Disseminate IAW the provisions of DoD Directive 5230.25 and AFI 61-204.

DESTRUCTION NOTICE - For classified documents, follow the procedures in DoD 5200.22-M, Industrial Security Manual, Section II-19 or DoD 5200.1-R, Information Security Program Regulation, Chapter IX. For unclassified, limited documents, destroy by any method that will prevent disclosure of contents or reconstruction of the document.

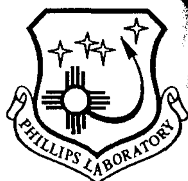

PHILLIPS LABORATORY
Space and Missiles Technology Directorate
AIR FORCE MATERIEL COMMAND
KIRTLAND AIR FORCE BASE, NM 87117-5776

UNCLASSIFIED

AD NUMBER

AD-B207 581

NEW LIMITATION CHANGE

TO

DISTRIBUTION STATEMENT A -
Approved for public release; Distribution unlimited.

Limitation Code: 1

FROM

DISTRIBUTION STATEMENT -

Limitation Code:

AUTHORITY

Janet E. Mosher; Phillips Lab/CA, Kirtland AFB, N.M.

THIS PAGE IS UNCLASSIFIED

PL-TR-95-1123

This final report was prepared by AstroPower, Inc., Newark, DE, Contract F29601-93-C-0188 Job Order, 3005C0DB, with Phillips Laboratory, Kirtland Air Force Base, New Mexico. The Laboratory Project Officer-in-Charge was Lt Dave Keener (VTP)

When Government drawings, specifications, or other data are used for any purpose other than in connection with a definitely Government-related procurement, the United States Government incurs no responsibility or any obligation whatsoever. The fact that the Government may have formulated or in any way supplied the said drawings, specifications, or other data, is not to be regarded by implication, or otherwise in any manner construed, as licensing the holder, or any other person or corporation; or as conveying any rights or permission to manufacture, use, or sell any patented invention that may in any way be related thereto.

This report has been authored by a contractor of the United States Government. Accordingly, the United States Government retains a nonexclusive royalty-free license to publish or reproduce the material contained herein, or allow others to do so, for the United States Government purposes.

This report contains proprietary information and shall not be either released outside the government, or used, duplicated or disclosed in whole or in part for manufacture or procurement, without the written permission of the contractor. This legend shall be marked on any reproduction hereof in whole or in part.

If your address has changed, if you wish to be removed from the mailing list, or if your organization no longer employs the addressee, please notify PL/VTP, 3550 Aberdeen Ave SE, Kirtland AFB, NM 87117-5776 to help maintain a current mailing list.

This report has been reviewed and is approved for publication.

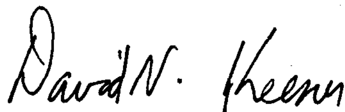

DAVE KEENER, Lt, USAF
Project Officer

FOR THE COMMANDER

DAVID KRISTENSEN, Lt Col, USAF
Chief, Space Power and Thermal
Management Division

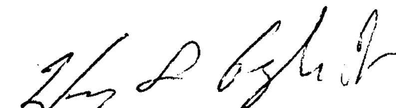

HENRY L. PUGH, JR., Col, USAF
Director of Space and Missiles Technology

DO NOT RETURN COPIES OF THIS REPORT UNLESS CONTRACTUAL OBLIGATIONS OR NOTICE ON A SPECIFIC DOCUMENT REQUIRES THAT IT BE RETURNED.

The following notice applies to any unclassified (including originally classified and now declassified) technical reports released to "qualified U.S. contractors" under the provisions of DoD Directive 5230.25, Withholding of Unclassified Technical Data From Public Disclosure.

NOTICE TO ACCOMPANY THE DISSEMINATION OF EXPORT-CONTROLLED TECHNICAL DATA

1. Export of information contained herein, which includes, in some circumstances, release to foreign nationals within the United States, without first obtaining approval or license from the Department of State for items controlled by the International Traffic in Arms Regulations (ITAR), or the Department of Commerce for items controlled by the Export Administration Regulations (EAR), may constitute a violation of law.

2. Under 22 U.S.C. 2778 the penalty for unlawful export of items or information controlled under the ITAR is up to two years imprisonment, or a fine of $100,000, or both. Under 50 U.S.C., Appendix 2410, the penalty for unlawful export of items or information controlled under the EAR is a fine of up to $1,000,000, or five times the value of the exports, whichever is greater; or for an individual, imprisonment of up to 10 years, or a fine of up to $250,000, or both.

3. In accordance with your certification that establishes you as a "qualified U.S. Contractor", unauthorized dissemination of this information is prohibited and may result in disqualification as a qualified U.S. contractor, and may be considered in determining your eligibility for future contracts with the Department of Defense.

4. The U.S. Government assumes no liability for direct patent infringement, or contributory patent infringement or misuse of technical data.

5. The U.S. Government does not warrant the adequacy, accuracy, currency, or completeness of the technical data.

6. The U.S. Government assumes no liability for loss, damage, or injury resulting from manufacture or use for any purpose of any product, article, system, or material involving reliance upon any or all technical data furnished in response to the request for technical data.

7. If the technical data furnished by the Government will be used for commercial manufacturing or other profit potential, a license for such use may be necessary. Any payments made in support of the request for data do not include or involve any license rights.

8. A copy of this notice shall be provided with any partial or complete reproduction of these data that are provided to qualified U.S. contractors.

D E S T R U C T I O N   N O T I C E

For classified documents, follow the procedures in DoD 5200.22-M, Industrial Security Manual, Section II-19 or DoD 5200.1-R, Information Security Program Regulation, Chapter IX. For unclassified, limited documents, destroy by any method that will prevent disclosure of contents or reconstruction of the document.

REPORT DOCUMENTATION PAGE

Form Approved
OMB No. 0704-0188

Public reporting burden for this collection of information is estimated to average 1 hour per response, including the time for reviewing instructions, searching existing data sources, gathering and maintaining the data needed, and completing and reviewing the collection of information. Send comments regarding this burden estimate or any other aspect of this collection of information, including suggestions for reducing this burden to Washington Headquarters Services, Directorate for Information Operations and Reports, 1215 Jefferson Davis Highway, Suite 1204, Arlington, VA 22202-4302, and to the Office of Management and Budget, Paperwork Reduction Project (0704-0188), Washington, DC 20503.

1. AGENCY USE ONLY *(Leave blank)*

2. REPORT DATE
5 Oct 95

3. REPORT TYPE AND DATES COVERED
4 Aug 93 - 3 Sept 95 Final Report

4. TITLE AND SUBTITLE
Lightweight, Light-trapped, Thin GaAs Solar Cells for Spacecraft Applications

5. FUNDING NUMBERS
C: F29601-93-C-0188
PE: 62601F
PR: 3005
TA: CO
WU: DB

6. AUTHOR(S)
Margaret H. Hannon, PRincipal Investigator

7. PERFORMING ORGANIZATION NAME(S) AND ADDRESS(ES)
AstroPower, Inc.
Solar Park
Newark, DE 19716-2000

8. PERFORMING ORGANIZATION REPORT NUMBER
API-0002Z

9. SPONSORING/MONITORING AGENCY NAME(S) AND ADDRESS(ES)
Phillips Laboratory
3550 Aberdeen Ave. SE
Kirtland AFB, NM 87117-5776

10. SPONSORING/MONITORING AGENCY REPORT NUMBER
PL-TR-95-1123

11. SUPPLEMENTARY NOTES

12a. DISTRIBUTION / AVAILABILITY STATEMENT
Distribution authorized to DoD components only; Proprietary Information; October 1995. Other requests shall be referred to AFMC/STI.

12b. DISTRIBUTION CODE

13. ABSTRACT *(Maximum 200 words)*

AstroPower has successfully demonstrated the potential performance of high specific power, ultra-thin GaAs solar cells by fabricating and testing ultra-thin, light-trapped, lightweight solar cell prototype devices. The development of lightweight, high performance GaAs solar cells that incorporate light trapping and possess inherent theoretical radiation tolerance is described. The incorporation of light trapping has increased the external quantum efficiency of these solar cells in the long wavelength range. Conversion efficiencies of 17.9% (AM0, 1X) were obtained from a 3 μm thick, 1 cm^2 solar cell. This results in a specific power of over 1020 W/kg (with a 3-mil cover slide) and a power density of 240 W/m^2. This technology can lead to the deployment of high performance, thin GaAs solar cells. The proposed solar cell design can have a significant impact on the longevity and power generation capabilities of space power supplies. The fabrication techniques developed here for GaAs can be applied to various other solar cell materials and designs including tandem solar cells and high voltage concentrator cells.

14. SUBJECT TERMS

15. NUMBER OF PAGES
52

16. PRICE CODE

17. SECURITY CLASSIFICATION OF REPORT	18. SECURITY CLASSIFICATION OF THIS PAGE	19. SECURITY CLASSIFICATION OF ABSTRACT	20. LIMITATION OF ABSTRACT
unclassified	unclassified	unclassified	SAR

NSN 7540-01-280-5500

Standard Form 298 (Rev. 2-89)
Prescribed by ANSI Std. Z39-18
298-102

GOVERNMENT PURPOSE LICENSE RIGHTS
(SBIR PROGRAM)

Contract Number: F29601-93-C-0188
Contractor: AstroPower, Inc.
Newark, DE 19716-20000

For a period of four (4) years after delivery and acceptance of the last deliverable item under the above contract, this technical data shall be subject to the restrictions contained in the definition of "Limited Rights" in DFARS clause at 252.227-7013. After the four-year period, the data shall be subject to the restrictions contained in the definition of "Government Purpose License Rights" in DFARS clause at 252.227-7013. The Government assumes no liability for unauthorized use or disclosure by others. This legend shall be included on any reproduction thereof and shall be honored only as long as the data continues to meet the definition on Government purpose license rights.

CONTENTS

1. INTRODUCTION 1
1.1 Benefits of the Technology 2
2. PHASE II OBJECTIVES 4
3. PHASE II RESEARCH RESULTS 5
3.1 Task 1. Refine and Improve the LPE growth layers for the thin GaAs solar cell structure... 5
3.1.1 Epitaxial Growth 5
3.1.2 Device Structure 6
3.1.3 Optimization of High Energy Spectral Response 8
3.2 Task 2. Invention of a novel n-type back contact. 11
3.3 Task 3. Incorporate light trapping. 14
3.4 Task 4. Develop fabrication processes for the thin, light trapped GaAs solar cell. 15
3.4.1 Fabrication Process 15
3.4.2 Anti-reflection Coating Optimization 16
3.4.3 Front lead attachment 17
3.4.4 Back lead attachment 17
3.4.5 Grid Design 18
3.5 Task 5. Characterize the thin, light trapped GaAs solar cell 20
3.6 Task 6. Sample and Device Fabrication 23
3.6.1 Fabrication of final prototype solar cell samples. 23
3.7 Task 7. Thermal Cycle Testing. 35
3.8 Task 8. Manufacturing feasibility study. 36
4. CONCLUSION 41
5. RECOMMENDATIONS 42
6. REFERENCES 42

FIGURES

FIGURE 1. Current-voltage characteristics for prototype device G13901A. 1
FIGURE 2. Photograph of the front and back surface of the ultra-thin, light trapped GaAs solar cell. 1
FIGURE 3. Specific power of candidate space solar cells. 3
FIGURE 4. Growth sequence for the ultra-thin, light trapped GaAs solar cells. 5
FIGURE 5. GaAs solar cell structure. 6
FIGURE 6. Cross-sectional photomicrograph of the device layers. 7
FIGURE 7. Electrochemical CV profile of beryllium diffused emitter region. 7
FIGURE 8. Comparison of the internal quantum efficiency of two LPE grown solar cells. 9
FIGURE 9. External quantum efficiency of a tin-doped device compared to a tellurium-doped device. 10
FIGURE 10. Current-voltage characteristics of a GaAs solar cell with a tin-doped GaAs base layer. 10
FIGURE 11. Contact resistance of AuGeNi contacts annealed at various temperatures (Ref. 6). 11
FIGURE 12. Ultra-thin solar cell after 280°C thermal anneal in forming gas and after plasma assisted anneal in hydrogen atmosphere. 13
FIGURE 13. Absorption results. 14
FIGURE 14. External quantum efficiency curve for device G13405B. 15
FIGURE 15. Back contact structure for the thin, GaAs solar cell prototypes. 16
FIGURE 16. Layer thicknesses and refractive indices for optimized anti-reflection coating. 16
FIGURE 17. Gray JV data for a high leakage and low leakage GaAs solar cell. 22
FIGURE 18. Current-voltage characteristics for deliverable G13506D. 25
FIGURE 19. External quantum efficiency of deliverable G13506D. 25
FIGURE 20. Current-voltage characteristics for deliverable G13601C. 26
FIGURE 21. External quantum efficiency for deliverable G13601C. 26
FIGURE 22. Current-voltage characteristics for deliverable G13601E. 27
FIGURE 23. External quantum efficiency curve for deliverable G13601E. 27
FIGURE 24. Current-voltage characteristics for deliverable G13901A. 28
FIGURE 25. External quantum efficiency for deliverable G13901A. 28
FIGURE 26. Current-voltage characteristics for deliverable G13901C. 29
FIGURE 27. External quantum efficiency for deliverable G13901C. 29
FIGURE 28. Current-voltage characteristics for deliverable G13901E. 30
FIGURE 29. External quantum efficiency for deliverable G13901E. 30
FIGURE 30. Current-voltage characteristics for deliverable G13905F. 31
FIGURE 31. External quantum efficiency for deliverable G13905F. 31
FIGURE 32. Current-voltage characteristics for deliverable G13906A. 32
FIGURE 33. External quantum efficiency for deliverable G13906A. 32
FIGURE 34. Current-voltage characteristics for deliverable G13912A. 33
FIGURE 35. External quantum efficiency for deliverable G13912A. 33
FIGURE 36. Current-voltage characteristics for deliverable G13912B. 34
FIGURE 37. External quantum efficiency curve for deliverable G13912B. 34
FIGURE 38. High temperature current-voltage characteristics of GaAs solar cell G14002. 36

TABLES

TABLE 1. Reference data compared to electrochemical CV profile measurements of AstroPower's devices. 8

TABLE 2. Diffusion and dopant concentration parameters. 8

TABLE 3. Electrical characteristics of tin and tellurium solar cells on a substrate. 11

TABLE 4. Metal systems investigated for ohmic contact to n-type GaAs. 12

TABLE 5. Reflection loss before and after optimized AR is applied. 17

TABLE 6. Optimized emitter and base region parameters. 19

TABLE 7. Parameter definitions for grid design calculations. 20

TABLE 8. Leakage currents of some of the GaAs solar cells measured during the Phase II program. 22

TABLE 9. Current-voltage characteristics of six 1 cm^2 devices fabricated from one large area ($8cm^2$) LPE growth. 23

TABLE 10. Electrical Characteristics of ten best effort light-trapped, thin GaAs solar cells. 24

TABLE 11. Comparison of solar cell electrical performance before and after 100 thermal cycles. 35

1. INTRODUCTION

AstroPower has successfully demonstrated the potential performance of high specific power, ultra-thin GaAs solar cells by fabricating and testing prototype devices. This report describes the development of lightweight, high performance GaAs solar cells that incorporate light trapping and possess inherent theoretical radiation tolerance. Ultra-thin, light-trapped solar cells have been fabricated and the light trapping demonstrated. Conversion efficiencies of 17.9% (AM0, 1X) were obtained from a 3 μm thick, 1 cm^2 solar cell. This results in a specific power of over 1020 W/kg (with a 3-mil cover slide) and a power density of 240 W/m^2. The current-voltage characteristics of this device are shown in Figure 1. Photographs of a prototype solar cell are shown in Figure 2. The front surface is shown in Figure 2a and the back surface, including the n-type contacts and silver reflector, is shown in Figure 2b.

sample	G13901A
Voc	1.015 V
Jsc	29.54 mA/cm^2
Fill Factor	80.3%
Area	1 cm^2
Thickness	3 μm
AM0, 1X efficiency	17.9%

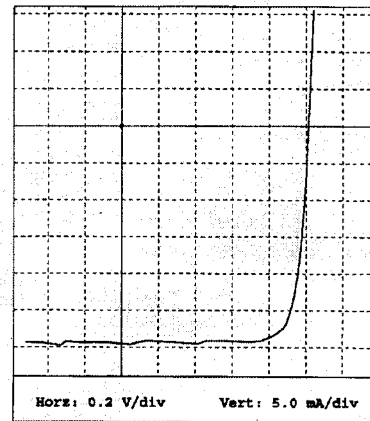

FIGURE 1. Current-voltage characteristics for prototype device G13901A.

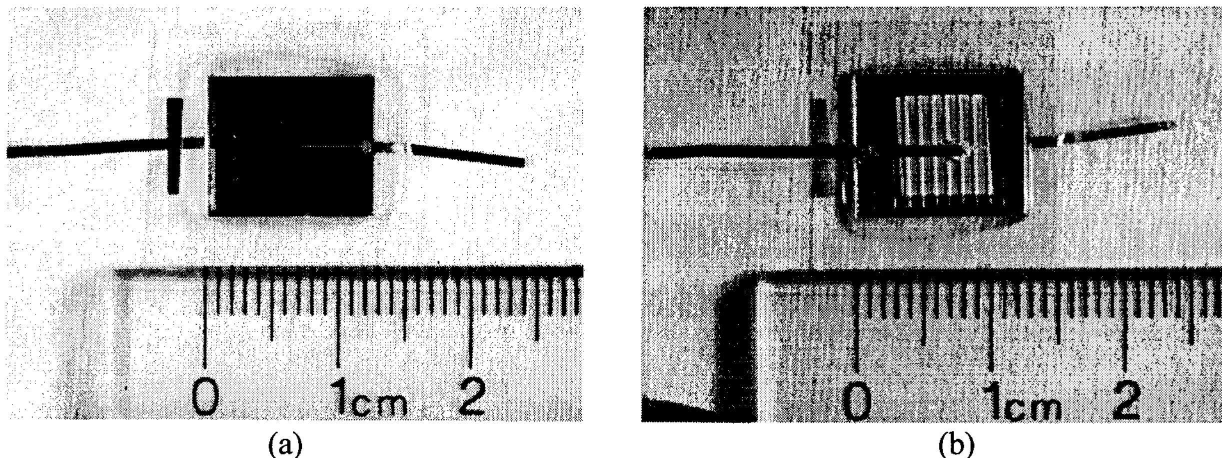

FIGURE 2. Photograph of the front (a) and back (b) surface of the ultra-thin, light trapped GaAs solar cell.

This technology can lead to the deployment of high performance, thin GaAs solar cells. This solar cell design will have a significant impact on the longevity and power generation capabilities of space power supplies. The fabrication technology developed here for GaAs can be applied to various other solar cell materials and designs including tandem solar cells and high voltage concentrator cells.

1.1 Benefits of the Technology

The high performance benefits of the ultra-lightweight, thin, light-trapped GaAs solar cell design meets the technology demanded for solar space power with increased performance as required for the space cell industry (Ref. 1). This solar cell design incorporates several features that lead to:

- **higher open circuit voltage**
  - reduced recombination volume
  - AlGaAs passivated surfaces
  - highly doped base region
- **higher short circuit current**
  - light trapping by a textured, reflecting back surface
- **superior radiation tolerance**
  - minimal dependence of solar cell performance on diffusion length
- **higher specific power**
  - thin, lightweight array
  - high efficiency device design

Direct bandgap materials such as GaAs make excellent candidates for thin devices. A high photon absorption coefficient for light of an energy greater than the bandgap of such materials makes it possible to fabricate cells in which the thickness of the active region is considerably smaller than that in indirect materials. Light of photon energy greater than the bandgap is absorbed within the first few microns of a direct bandgap semiconductor. Conventional high performance GaAs solar cells are usually comprised of epitaxial layers of GaAs and $Al_xGa_{(1-x)}As$ formed on a GaAs or Ge substrate. When GaAs devices are fabricated on a thick substrate, the substrate acts only as a support and does not contribute to the overall performance of the device.

The advantages gained from fabricating thin solar cells include a high power-to-weight ratio (specific power) which is important for space applications (Ref. 2). In addition, without a GaAs substrate the free carrier absorption is minimized and a light trapped device becomes feasible. Light trapping increases the effective optical path length with the use of a reflector and/or a textured surface. Incorporating light trapping into the device increases the performance by increasing the short circuit current, while the reduced GaAs base thickness lowers the reverse saturation current. Both of these effects enhance the open circuit voltage (Ref. 3).

Because the device is thin, back surface recombination becomes an important issue. Recombination of the carriers at the back surface is reduced by incorporating an $Al_xGa_{1-x}As$ ($x > 0.5$) back surface passivation layer. A metal mirror is deposited over the back AlGaAs layer to reflect longer wavelength light back into the base, thus doubling the effective absorption volume of the device. The front surface is also passivated by an $Al_xGa_{1-x}As$ ($x = 0.85$) layer which is well known to improve the efficiency of this type of cell.

The high efficiency and light weight of the cover glass supported GaAs solar cell can have a significant impact on space solar array technology. Figure 3 shows the specific power and power density of several candidate solar cells. The thin GaAs solar cell design offers a 440% increase in specific power compared to a 14.5% efficient silicon solar cell. The power to weight ratio is calculated assuming there is a 3-mil cover glass and 1-mil silicone adhesive on the front surface of the GaAs solar cell.

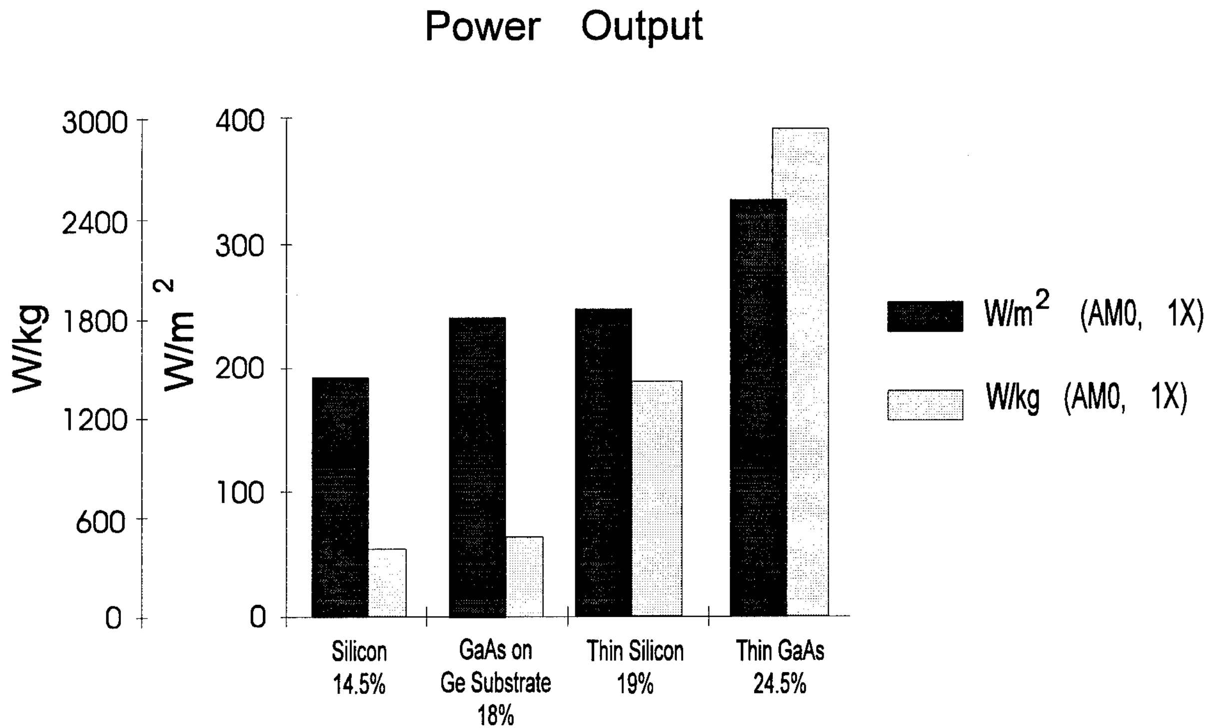

FIGURE 3. Specific power of candidate space solar cells.

The results of the Phase II program have demonstrated the feasibility of the ultra-lightweight, thin, light trapped GaAs solar cell for advanced space power systems. The incorporation of light trapping has increased the external quantum efficiency of these solar cells in the long wavelength range. Prototype devices were fabricated and tested with efficiencies as high as 17.9 % (AM0, 1X) for a 3 μm thick, 1 cm^2 solar cell. This results in a specific power of 1020 W/kg (with a 3-mil cover slide) and a power density of 240 W/m^2. This technology will result in a revolutionary improvement in survivability, performance, and manufacturability of lightweight GaAs solar cell products for future Earth-orbiting science and space exploration missions.

2. PHASE II OBJECTIVES

The overall objective of the Phase II program was the demonstration of the thin, light-trapped, GaAs space solar cell as a potential high performance solar power conversion device.

The specific research tasks and accomplishments were:

1. Refine and improve the LPE growth layers for the thin GaAs solar cell structure.
   - ☑ 0.3 μm, $1.5 \times 10^{18} cm^{-3}$ Be diffused emitter
   - ☑ 2 μm, $2 \times 10^{17} cm^{-3}$ GaAs base layer
   - ☑ 7% gain in short circuit current due to optimized high energy response
   - ☑ 18.4% conversion efficiency from improvement in spectral response
2. Invention of a novel n-type back contact.
   - ☑ Invented plasma assisted annealing technique
   - ☑ fill factor increase from 68% to 78%
   - ☑ fill factor of 80.3% for the ultra-thin, light-trapped GaAs solar celll
3. Incorporate light trapping.
   - ☑ external quantum efficiency at 850 nm increased by 5.2%
4. Develop fabrication processes for the thin, light-trapped GaAs solar cell.
   - ☑ front and back lead attachment with no device degradation
   - ☑ losses due to grid shading and series resistance total 5%
5. Characterize the thin, light-trapped GaAs solar cell.
   - ☑ $J_{01} = 3 \times 10^{-19}$ A/cm^2 and $J_{02} = 3 \times 10^{-11}$ A/cm^2
   - ☑ Voc = 1.015 V, Jsc = 29.54 mA/cm2, Fill Factor = 80.3% for a conversion efficiency of 17.9%
6. Sample and device fabrication.
   - ☑ median device efficiency of 17.14% for six 1 cm2 devices fabricated from one large area (8cm2) LPE growth
   - ☑ delivered ten prototype solar cells
7. Thermal cycle testing.
   - ☑ 100 thermal cycles from -80°C to +120°C resulted in no degradation.
   - ☑ evaluated current-voltage characteristics at elevated temperatures
8. Manufacturing feasibility study.
   - ☑ $416/Watt fully loaded costs for 25-cm^2 cells at greater than 100 cells/month
   - ☑ present production capacity of 800 wafers/month using existing facility

3. PHASE II RESEARCH RESULTS

3.1 Task 1. Refine and Improve the LPE growth layers for the thin GaAs solar cell structure.

3.1.1 Epitaxial Growth

Devices were grown by the method of liquid phase epitaxy (LPE). LPE is a single crystal growth technique, in which a layer grows from a supersaturated liquid metal solution onto a single crystal substrate which must have a crystalline structure similar to that of the grown layer. In III-V film growth, the group III metal component is typically used as the solvent and the group V component (solute) is incorporated by dissolving III-V polycrystalline source material into the solution at or above the growth temperature. The sliding (Ref. 4) method of LPE was used, where the melt solutions are held in stationary crucibles, and the substrate material is slid under the growth melts. The growth system components are made from high purity graphite and quartz to limit unintentional impurity incorporation into the semiconductor films.

The gallium solvent was prebaked for 12 to 15 hours at 880°C in a Pd-purified hydrogen atmosphere to remove impurities. A quantity of 22 grams of Ga was used for each of the three growth melts. After loading the substrate and melt constituents, the system was flushed with N_2, evacuated to less than 100 μm-Hg, and backfilled with Pd-purified H_2. The growth sequence for the solar cells fabricated during this program is shown in Figure 4. After completing the growth sequence, the boat was cooled to room temperature and the system was flushed with N_2. The boat was then removed from the system and unloaded.

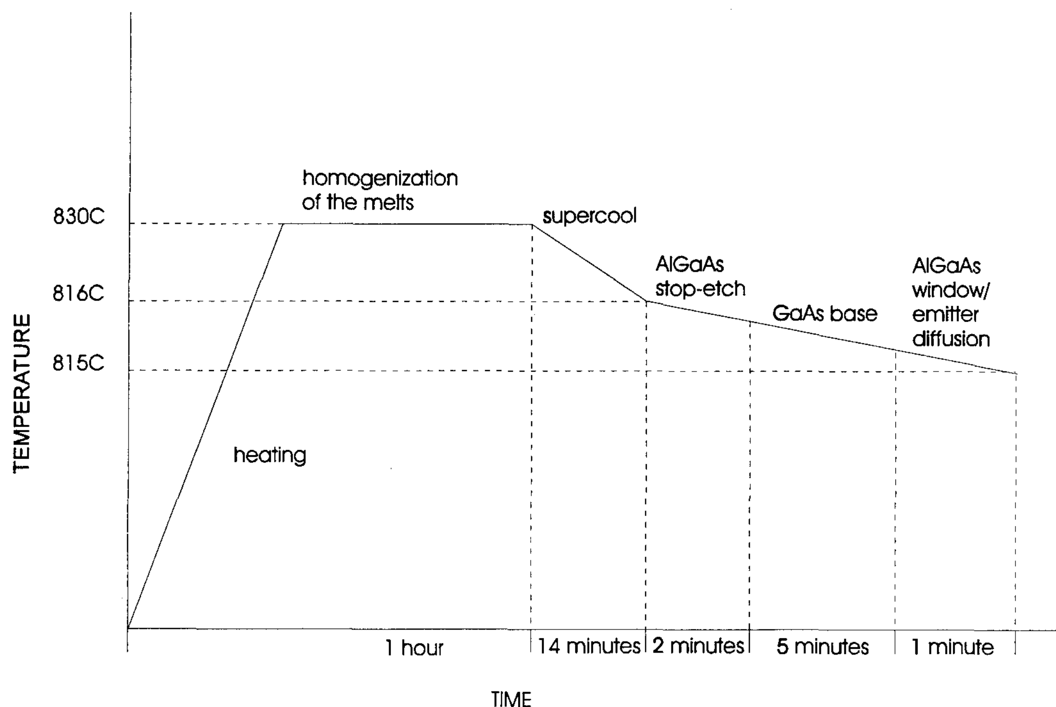

FIGURE 4. Growth sequence for the ultra-thin, light trapped GaAs solar cells.

3.1.2 Device Structure

The GaAs solar cell structure consists of an n-type $Al_{.60}Ga_{.40}As$ stop-etch layer, an n-type GaAs base layer, and a p-type $Al_{.85}Ga_{.15}As$ passivation or window layer. The p-type GaAs emitter is diffused during the growth of the $Al_{.85}Ga_{.15}As$ passivation layer. The structure of the epitaxial layers is displayed in Figure 5.

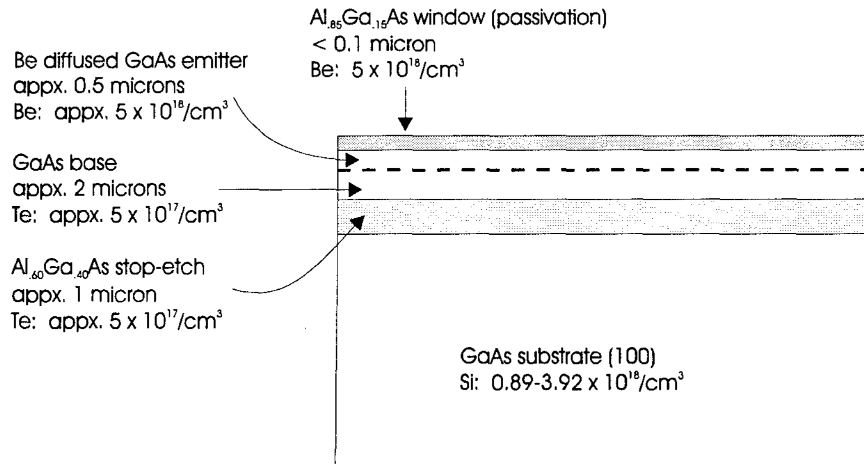

FIGURE 5. GaAs solar cell structure.

The substrate was n-type, GaAs (Si: $1\text{-}3\times10^{18}cm^{-3}$) oriented on the (100) plane. The substrate dimensions were $2.5\times4.5cm^2$. The growth layers consisted of the $Al_{.60}Ga_{.40}As$ n-type stop-etch layer, the n-type GaAs base layer, and the p-type $Al_{.85}Ga_{.15}As$ passivation or window layer. During the window layer growth, the p-type dopant (Be) diffuses into the n-type base layer, forming the p-type GaAs emitter.

A cross-sectional photograph of the device layers is shown in Figure 6. The AlGaAs stop-etch layer was 1 μm thick and the GaAs base and emitter thickness totaled 3 μm. The p-n junction depth is not visible on the photograph, nor is the $Al_{.85}Ga_{.15}As$ passivation layer. However, electrochemical capacitance-voltage (C-V) profiles of the solar cell structures provide information on the p-n junction depth. These measurements were performed on the GaAs solar cell structure by Bio-Rad Semiconductor in Mountain View, California. Window layer growth/diffusion times of 10, 20, and 60 seconds were profiled. The results of the 60 second diffusion time are shown in Figure 7. The emitter depth is 0.25 to 0.3 microns and the emitter carrier concentration is approximately $1.5\times10^{18}/cm^3$. The n-type GaAs base has a carrier concentration of approximately $2\times10^{17}/cm^3$. The p-n junction is relatively abrupt, which is desirable for increased device performance. With an abrupt junction, the reverse leakage current due to recombination in the depletion region is reduced and the breakdown in reverse bias is much sharper. A p-n junction with an abrupt interface shows reduced interface leakage.

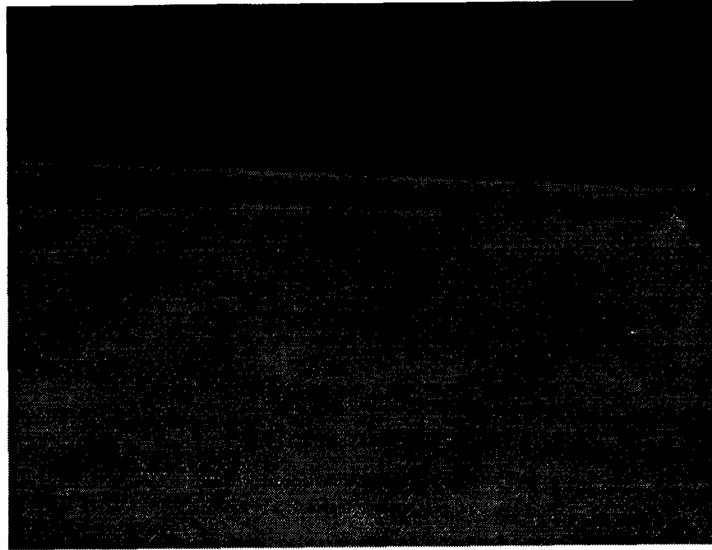

FIGURE 6. Cross-sectional photomicrograph of the device layers for the ultra-thin GaAs solar cell (G13813, 1000X).

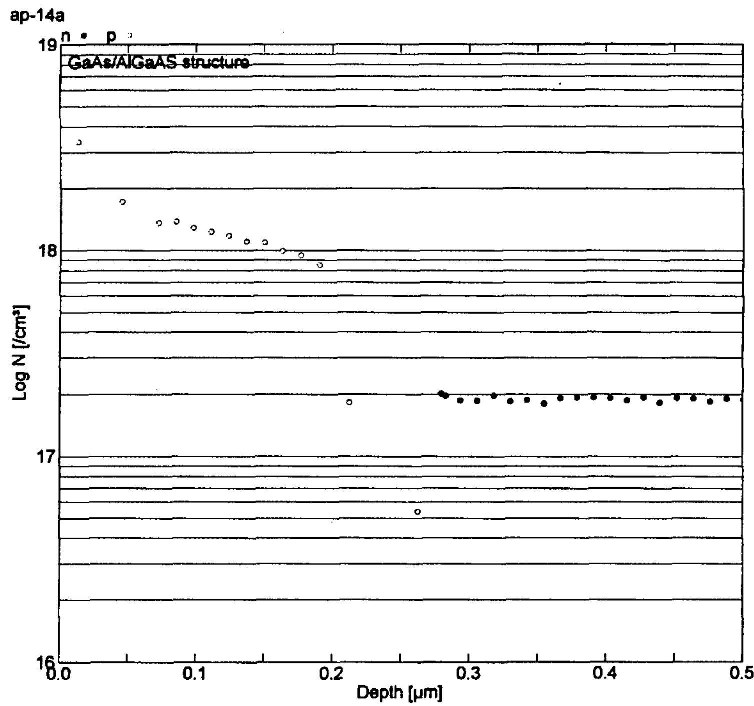

FIGURE 7. Electrochemical CV profile of beryllium diffused (60 second) emitter region.

The results of the measurements of AstroPower's samples are compared to the data of reference 5 in Table 1. Our data correlate with their results for the diffusion of beryllium from an LPE melt into n-doped GaAs at 800°C.

TABLE 1. Reference data compared to electrochemical CV profile measurements of AstroPower's devices.

	Reference data (Ref. 5)	Measured data (AstroPower material)
Be concentration	0.01 atomic %	0.01%
Time	1 minute	1 minute
Temperature	800°C	830°C
Carrier concentration	$2.5x10^{18}/cm^3$	$1.5x10^{18}/cm^3$
Depth	0.20μm	0.26μm
Sheet resistance	1000Ω	1000Ω

3.1.3 Optimization of High Energy Spectral Response

Emitter diffusion experiments were conducted in an effort to increase the short circuit current of the thin GaAs solar cell. Quantum efficiency curves indicated poor collection efficiencies for minority carriers generated near the front surface. The loss currents of these cells ($J_{01}=3x10^{-19}$ A/cm^2 and $J_{02}=5x10^{-11}$ A/cm^2) approach the theoretical minimum for GaAs.

Reducing the diffusion time from 120 seconds to 10 seconds and reducing the beryllium concentration in the gallium melt from 0.04 to 0.01 atomic percent significantly improved the high energy or blue response of the GaAs solar cell (Table 2). Figure 8 compares the internal quantum efficiencies of two different LPE grown solar cells. The gain in available short circuit current due to the improved blue response was 2.1 mA/cm^2, a gain of 7%. These quantum efficiency data were measured before the devices were thinned (GaAs substrate removed) and bonded to glass.

TABLE 2. Diffusion and dopant concentration parameters for the solar cells depicted in Figure 8.

sample	diffusion time (seconds)	beryllium concentration (at%)
G13405D	120	0.04
G13705D	10	0.01

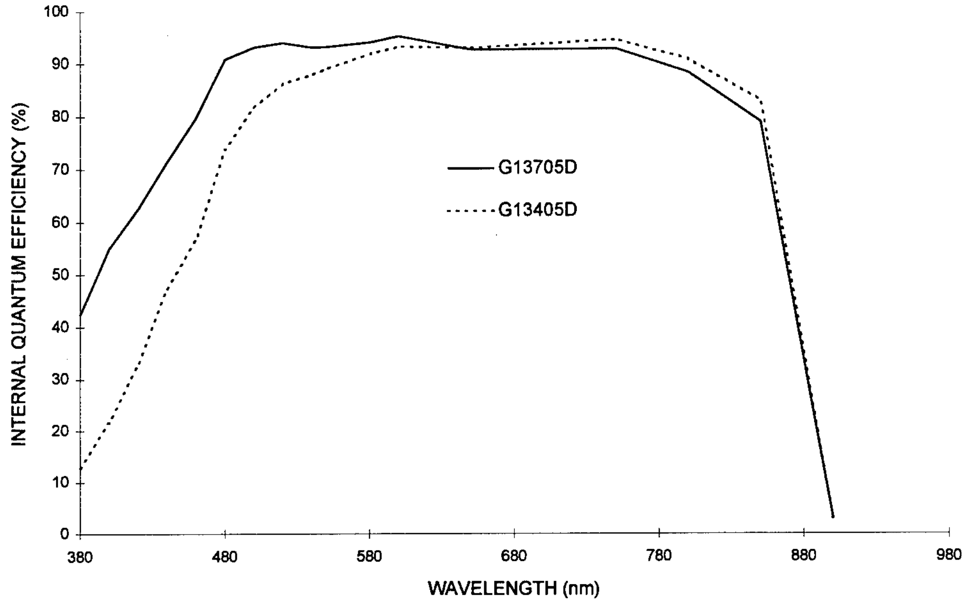

FIGURE 8. Comparison of the internal quantum efficiency of two LPE grown solar cells. The diffusion and dopant parameters are shown in Table 2.

The typical value for surface recombination velocity for an ideal AlGaAs/GaAs interface is 1000 cm/sec (Ref. 6). The $Al_{.85}Ga_{.15}As$ passivation layer provides surface passivation for the thin GaAs solar cell and assures that the surface recombination velocity should be comparable to this value. Potential reasons for the improved high energy response include a thinner emitter, a thinner $Al_{.85}Ga_{.15}As$ passivation layer, and/or increased lifetimes in the emitter. We believe that the improved high energy response is the result of reducing the emitter doping by a factor of four, yielding longer emitter lifetimes and increased diffusion lengths. Confirmation of this effect would involve a detailed study.

Base Dopant

The AlGaAs stop-etch layer and GaAs base layer of the GaAs solar cell are n-type. Devices were completed using Te as the impurity dopant for these layers, and also using Sn as the impurity dopant for the GaAs base layer with an undoped AlGaAs stop-etch layer. Although efficiencies exceeding 17% were obtained for both cases, the external quantum efficiency of the Sn doped ($Nd = 2x10^{17}cm^{-3}$) structures was significantly higher in the long wavelength region (600 to 870 nm) as shown in Figure 9. Varying light intensity I-V measurements indicate low leakage current densities ($J_{01} = 3.5x10^{-19}$ A/cm^2, $J_{02} = 3x10^{-11}$ A/cm^2). The short circuit current density of the tin doped cells is approximately 1 mA/cm^2 greater than the average tellurium doped cells. Open circuit voltages were slightly increased due to the increased short circuit current and decreased leakage current. The current-voltage characteristics of a tin doped solar cell are shown in Figure 10. A comparison of the electrical characteristics for tin and tellurium doped solar cells is presented in Table 3.

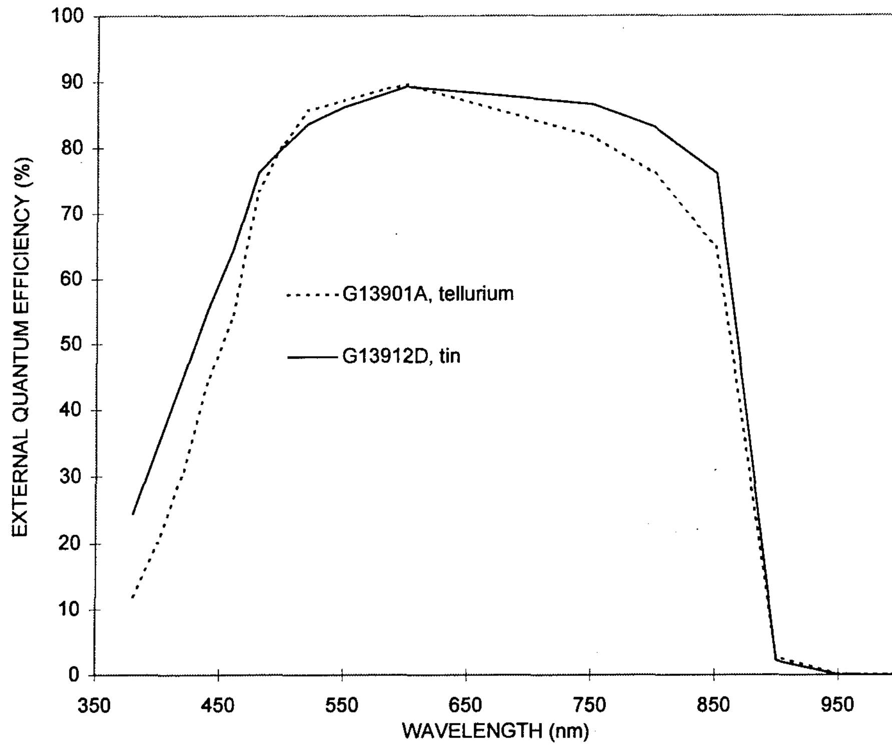

FIGURE 9. External quantum efficiency of a tin-doped (G13912D) device compared to a tellurium-doped (G13901A) device.

sample	G13912D
Voc	1.016 V
Jsc	30.83 mA/cm^2
Fill Factor	79.3 %
Area	1 cm^2
Thickness	on GaAs substrate
AM0, 1X efficiency	18.4 %

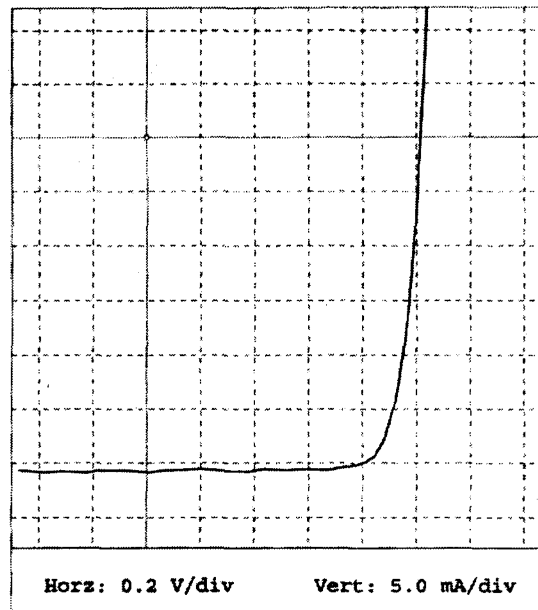

FIGURE 10. Current-voltage characteristics of a GaAs solar cell with a tin-doped GaAs base layer (G13912D).

TABLE 3. Electrical characteristics of tin and tellurium solar cells on a substrate.

sample	Voc (V)	Jsc (mA/cm^2)	FF (%)	J_{01} (A/cm^2)	J_{02} (A/cm^2)	Efficiency (%)
G13912B (Sn)	1.019	30.35	78.2	3.0×10^{-19}	5×10^{-11}	18.0
G13912D (Sn)	1.016	30.83	79.3	3.5×10^{-19}	3×10^{-11}	18.4
G13901A (Te)	1.010	29.00	79.0	5.0×10^{-19}	8×10^{-10}	17.1

3.2 Task 2. Invention of a novel n-type back contact.

An ohmic contact is a metal-semiconductor contact that has a negligible contact resistance relative to the bulk or spreading resistance of the semiconductor (Ref. 7). An ohmic metal-semiconductor contact has a linear I-V characteristic in both biasing directions. AuGeNi contacts are the most common for fabricating ohmic contact to n-type GaAs. This contact system typically requires annealing temperatures above 360°C for ohmic behavior, and above 440°C for the lowest contact resistance. Figure 11 shows the dependence of contact resistance on annealing temperature. The contact resistance is also influenced by the GaAs substrate surface cleaning procedure, deposition sequence/layer thickness, and the annealing method/temperatures (Ref. 6).

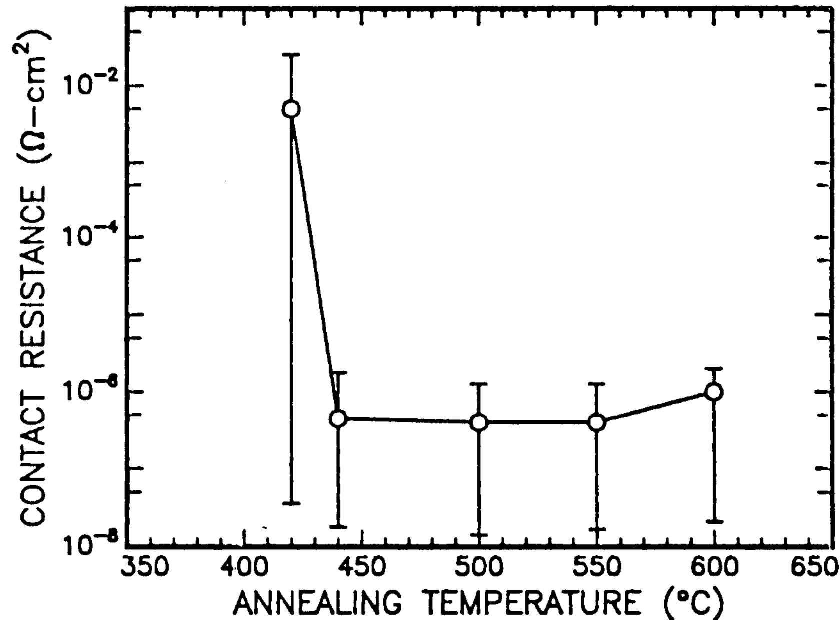

FIGURE 11. Contact resistance of AuGeNi contacts annealed at various temperatures (Ref. 6).

For the ultra-thin, light-trapped, adhesive bonded GaAs solar cells, the thermal mismatch between the GaAs and the silicone adhesive limits the temperature the GaAs/silicone adhesive may encounter during the post-contact heat treatment. This temperature limit resulted in series resistance losses and/or blocking contacts in the solar cell due to a high contact resistance at the nonalloyed base contacts. The effect of the contact resistance varied between solar cells when

the same deposition and heat treatment sequences were used, most likely due to slight variations in the surface preparation and the GaAs carrier concentration.

Table 4 reviews some of the metal systems for ohmic contact to n-type GaAs investigated during the Phase I program and the resulting pad-to-pad resistance. The contact structures were deposited in random pads and the resistance was measured from pad-to-pad. This is a qualitative measurement that indicates the feasibility of a particular contact structure. The carrier concentration of the layer contacted was $1\text{-}5\times10^{17}/cm^3$. Although the Sn/Ni/Au system with no alloy produced results comparable to the Au/Ge/Au/Ni system with a 475°C alloy, the results were not consistent.

TABLE 4. Metal systems investigated for ohmic contact to n-type GaAs.

Contact metal and thickness (Å)	alloy time (min.)/temperature (°C)	pad-to-pad resistance (Ω)
300Au/725Ge/1160Au/500Ni	none	1.6×10^6
	2/475	2
100Sn/300Ni/1000Au	none	19-59
	0.5/150	20 - 72
100Sn/1000Au	none	31 - 847
	0.5/200	34 - 308
100Sn/100Ni/1000Au	none	21 - 49
100In/500Sn/500In/1000Au	none	14 - 68
	1/200	12 - 1383
100Ni/100Sn/300Ni/100Sn/	none	11 - 728
300Ni/100Sn/500Ni/1000Au	1/200	7 - 1714
100Au/200Ni/1000Au	none	1216 - 1498
	1/200	1661 - 2005
500Ge:In/1000Au	none	8×10^6 - $16\text{x}0^6$
	1/200	11×10^6 - 36×10^6
100Sn/500Ni/1000Au	none	9 - 3.5x106
	1/150	9 - 8x106
100Sn/500Ni/1000Au	none	4 - 9
100Sn/500Ni/1000Au	none	2×10^6 - 1.2×10^6
100Sn/500Ni/1000Au	none	29
100Sn/500Ni/1000Au	none	11
300Au/300Zn/1700Au	none	13.5

During the Phase II program, a new method of achieving ohmic contact to the n-type region was developed. This technique was more successful than conventional heating in forming gas. The method involved heating the solar cell to 300°C under hydrogen and introducing radio-frequency (RF) plasma in the chamber. It is suspected that the RF power heats the metal-semiconductor interface past 300°C, while keeping the GaAs adhesive interface below the critical temperature. This technique permits achievement of a low resistivity, ohmic contact to the solar cell. A significant increase in fill factor was observed using this method.

Figure 12 illustrates the effect of plasma assisted annealing after a thermal annealing step had failed. This technique increased the fill factor from 61% to 78%. The metal system was the standard Au/Ge/Au/Ni. The metal-semiconductor contact in Figure 12a is rectifying; there is a

larger barrier to charge carrier transport in one direction than in the opposite direction (Ref. 8). This is evidenced by the asymmetric, nonlinear current-voltage characteristic. The distinctive "nose" in the curve is due to a blocking contact. The alloy temperature was limited to 280°C due to the thermal expansion coefficient difference between the GaAs and the silicone adhesive.

The metal-semiconductor contact in Figure 12b is nonrectifying, meaning there is no effective barrier to charge carrier transport in either direction, as evidenced by the symmetric, linear I-V characteristic. The temperature of the silicone adhesive/GaAs interface was kept below the critical point for breakage in both annealing processes.

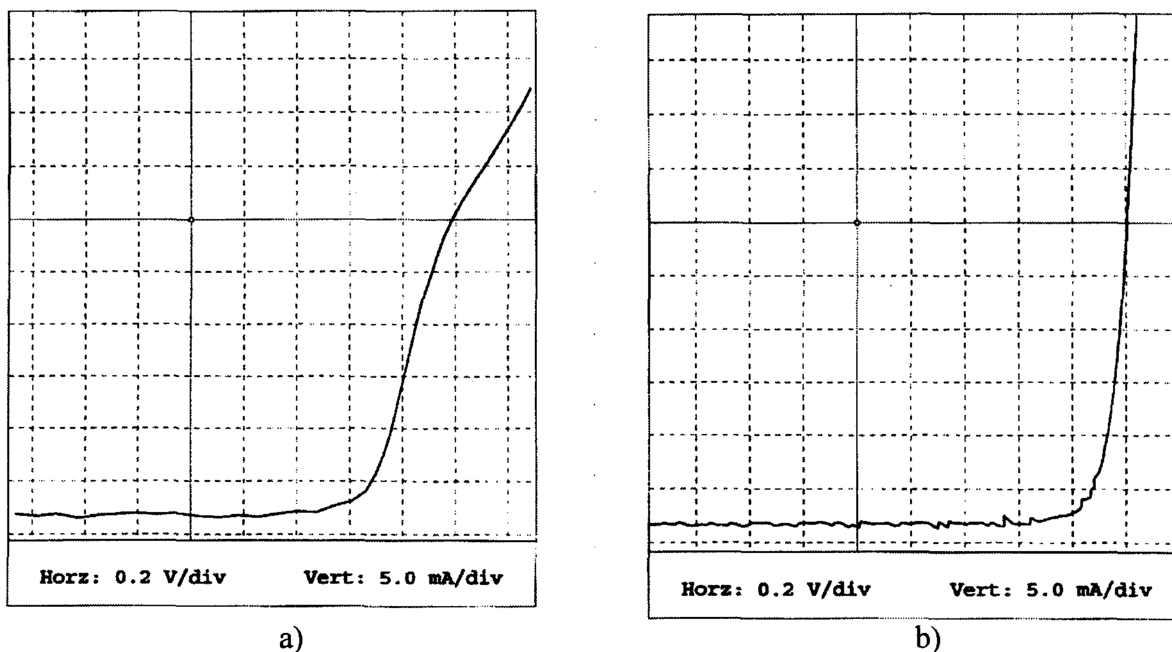

FIGURE 12. Ultra-thin solar cell G13601C a) after 280°C thermal anneal in forming gas (fill factor = 61%) and b) after plasma assisted anneal in hydrogen atmosphere (fill factor = 78%).

We have concluded that the plasma assisted annealing technique forms ohmic contact to n-type GaAs at a significantly lower temperature than standard alloy procedures, using the standard Au/Ge/Au/Ni metal system. This technology was successful for ultra-thin GaAs devices and could prove invaluable in the future for various space solar cell devices.

3.3 Task 3. Incorporate light trapping.

The Phase I program demonstrated light trapping of a GaAs LPE layer. Figure 13 shows absorption data from a 1.5 micron LPE layer i) before substrate removal, ii) after substrate removal, and iii) after substrate removal and addition of a back surface metal reflector. As expected, the amount of light absorbed decreases as the GaAs structure is thinned, particularly over the 550 nm to 850 nm range where there is a high flux density in the solar spectrum. Application of a silver back reflector increases the absorption due to a longer effective optical path length. The absorption curve closely matches that of the thin material on the GaAs substrate, with greater than 70% of the light absorbed over the 550 nm to 850 nm range. The values for absorption were calculated as (1 - (reflection + transmission)). These samples did not have an AR coating and therefore the average reflection loss was approximately 30%. Correcting the data for reflection losses increases the absorption for the thinned sample with a reflector to close to 100% over the 550 nm to 850 nm range.

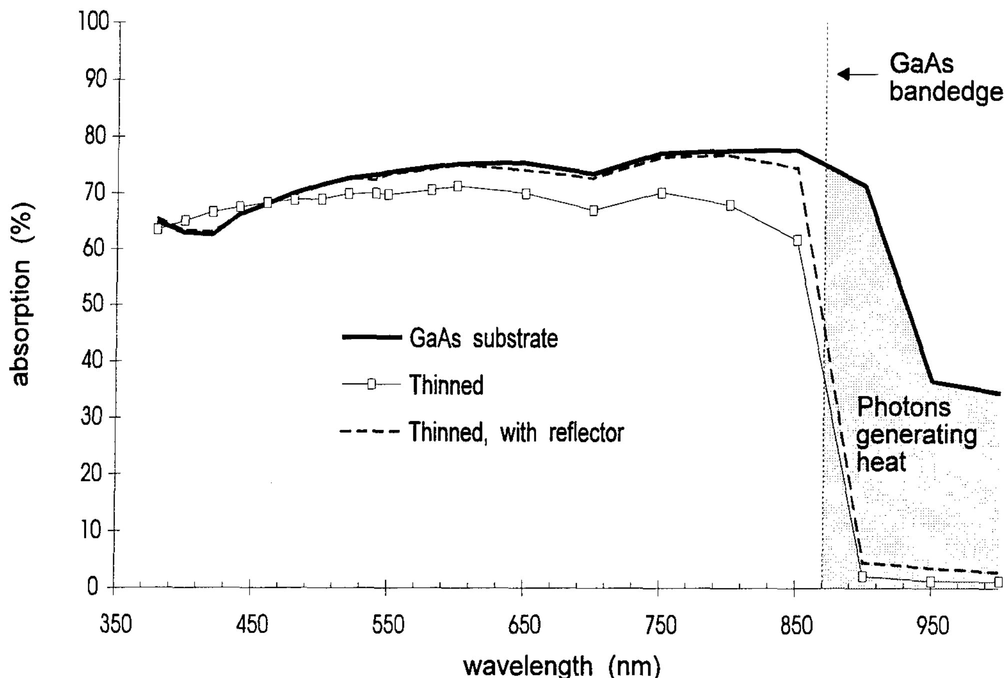

FIGURE 13. Absorption results for: 1.5 μm GaAs LPE layer on a GaAs substrate; 1.5 μm glass bonded GaAs layer; and glass bonded 1.5 μm GaAs layer with a reflector.

During the Phase II program, light trapping has been demonstrated on the ultra-thin GaAs solar cells. The external quantum efficiency curve illustrated in Figure 14 shows an increase in long wavelength response (between 650 and 870 nm) of the thinned solar cell with a back surface reflector, compared to the same device before the thinning procedure (on the GaAs substrate). The external quantum efficiency of this device was increased by 5.2% at 850 nm with the incorporation of a back surface reflector. The gain in short circuit current density for this solar cell is approximately 0.7 mA/cm^2. This gain is expected to increase as the active device thickness is decreased to less than 2 microns.

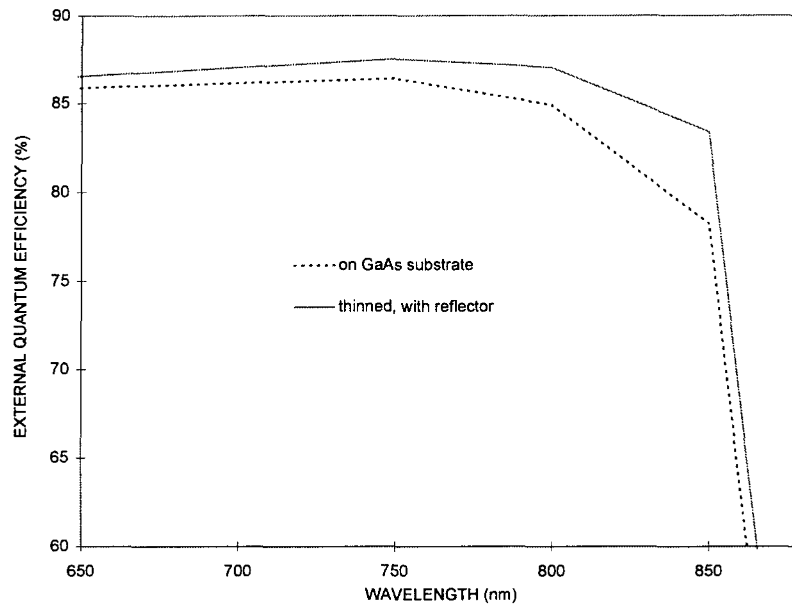

FIGURE 14. External quantum efficiency curve for device G13405B.

3.4 Task 4. Develop fabrication processes for the thin, light trapped GaAs solar cell.

3.4.1 Fabrication Process

The fabrication process for prototype devices is as follows (see Figure 15):

1. Grow solar cell layers on (100) GaAs, n-type (Si: $1\text{-}3\times10^{18}cm^{-3}$) substrate by LPE (see Section 3.1.1).
2. Pattern and deposit front, p-type contacts.
3. Pattern and electroplate high conductance, front, p-type contacts.
4. Thermosonic bond tab to front contact (see Section 3.4.3).
5. Deposit anti-reflection coating by plasma assisted CVD (see Section 3.4.2).
6. Adhesive bond the glass superstrate to the solar cell. A transparent, chemically resistant, silicone elastomer manufactured by Dow Corning (Sylgard) was used for bonding the solar cell to glass.
7. Chemically thin the GaAs substrate to less than 50μm using a hydrogen peroxide:ammonium hydroxide etch.
8. Using photolithography, protect areas of the substrate that will form the n-type contact layer.
9. Remove remainder of the GaAs substrate that is not protected with photoresist using the hydrogen peroxide:ammonium hydroxide selective etch.
10. Pattern and deposit back, n-type contacts on GaAs contact region.
11. Sinter the back contacts using the plasma assisted annealing process (see Section 3.2).
12. Deposit dielectric and metal reflector at the back surface.
13. Attach tab to the back of the solar cell using conductive epoxy (see Section 3.4.4).

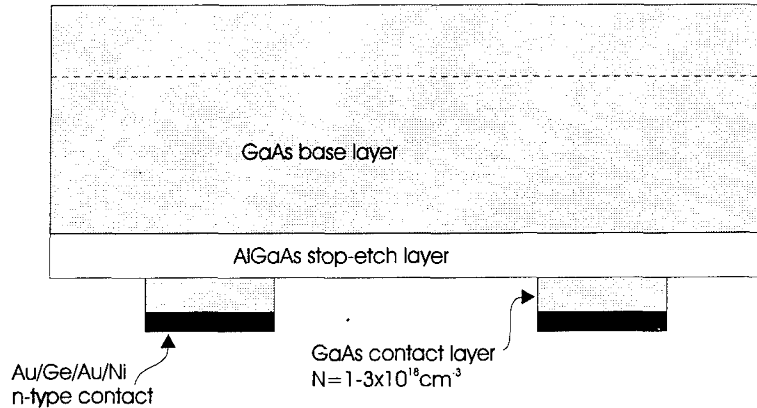

FIGURE 15. Back contact structure for the thin, GaAs solar cell prototypes.

3.4.2 Anti-reflection Coating Optimization

The anti-reflection coating was optimized so that the solar cell/silicone adhesive/glass interface exhibited minimal light reflection and the light generated current was maximized. Reflectance was modeled over the wavelength range of 400 nm to 881 nm. Reflectance minimums were found at each interface so that the short circuit current was maximized. The layer structure, along with the optimal thicknesses and refractive indices is shown in Figure 16.

Magnesium Flouride: 110 nm, n=1.38
CMG-150 coverglass: 150 um, n=1.52
Sylgard 182 silicone elastomer: 15um, n=1.43
Silicon Nitride: 70 nm, n=2.0
AlGaAs window x=0.8: 40nm, n=3.3
GaAs solar cell: 1-2 um, n=4.0

FIGURE 16. Layer thicknesses and refractive indices for optimized anti-reflection coating.

The current losses associated with reflection for a GaAs solar cell with the parameters displayed in Figure 16 are listed in Table 5. The optimized anti-reflection coating decreases reflection by 90%. Grid shading with our optimized front grid pattern is an additional 5%.

Table 5. Reflection loss before and after optimized AR is applied.

λ (nm)	400	440	500	540	581	650	700	750	800	850
Reflection loss before AR(%)	28	26	25	25	23	22	21	20	21	23
Reflection loss after AR (%)	5.9	3.3	1.9	1.6	1.4	1.5	1.8	2.4	3.3	4.1

3.4.3 Front lead attachment

Lead attachment to the emitter contact is achieved by thermosonic bonding a 25 micron thick gold ribbon to the gold plated contact pad. The process requires heating the cell to 150°C, then sonically "scrubbing" the ribbon into the gold contact pad. This method avoids the problems associated with soldering such as metallic leaching, scavenging, smearing and flux removal. Another benefit of the use of thermosonic or ultrasonic bonding technologies is that contact can be made to either a large pad or to thin metallic strips (Ref. 9). This is important for high efficiency solar cells because a large contact pad will reduce the short circuit current.

This method of lead attachment to the emitter caused no degradation to the solar cell performance. The current-voltage characteristics of the solar cells before and after thermosonic bonding were identical.

3.4.4 Back lead attachment

The back, n-type contact was tabbed using a single component silver epoxy. Initially, a low viscosity (10,000 cps) epoxy with a resistivity of $4\text{-}8 \times 10^{-3}$ ohm-cm was used. The low viscosity made it difficult to achieve a clean, small area tab to the back surface of the solar cell. Better results were obtained using an epoxy with a viscosity approximately five times higher (48,000 cps). This epoxy has a resistivity of approximately $1\text{-}5 \times 10^{-4}$ ohm-cm. Using this epoxy to attach the back contact lead to the thin solar cell caused no degradation to the fill factor and the thin solar cells also survived 100 thermal cycles from -80 to +120°C with no degradation (see Section 3.7).

An alternative to silver based epoxy is solder preforms. Indium bearing solders, silver solders, and gold-tin eutectic solders are used in the microelectronics industry for interconnecting circuit elements and chips. They are desirable when soldering to thin gold films because the effects of leaching (sold state diffusion of gold into the solder) and scavenging (molten solder dissolving the gold base) are minimized or eliminated compared to conventional tin-lead solders. Solder preforms offer the potential for minimizing the amount of material necessary for achieving proper adhesion and conduction. This material reduction would lower the specific weight of the thin solar cells. It is expected that the thin, light-trapped GaAs solar cells would be compatible with solder preforms and this alternative should be investigated in the future.

Thermosonic bonding of the back contact lead was not pursued because of the necessity of a thick, electroplated, gold layer on the back surface. This extra processing step increased the potential for shunt defects on the isolated devices. However, this technology would eliminate the

problems associated with epoxies such as outgassing. Thermosonic bonding was successful for the front lead attachment and caused no degradation of the device performance. Future work with the development of this approach, including space qualification, is recommended.

3.4.5 Grid Design

The thin, light-trapped GaAs solar cell was designed for high performance operation by simultaneously optimizing the diode junction parameters and physical dimensions. The three most relevant parameters for solar cell operation are open circuit voltage, short circuit current and fill factor. All three of these parameters are dependent on the diode's properties such as impurity doping, surface recombination, and lifetime, and on the physical geometry of both the collecting junction and electrical contacts.

The p-n junction solar cell's behavior can be predicted by the following equation:

$$I = I_o\left[e^{\frac{q(V-IR_s)}{kT}} - 1\right] + \frac{V - IR_s}{R_{sh}} - I_{ph}$$

where I and V are the terminal current and voltage respectively, I_0 is referred to as the reverse saturation current, I_{ph} is the light generated current and R_s and R_{sh} are the series resistance and the shunt resistance of the solar cell. For this model, it is assumed that current components such as space charge recombination current are negligible at one sun intensities.

Optimization of the above equation for solar cell p-n junction characteristics requires solving for values of reverse saturation current and light generated current simultaneously. It is desirable to minimize the reverse saturation current so that the open circuit voltage is high and the light generated current is maximized. Both of these parameters are functions of doping, junction depth, surface recombination, bulk lifetimes and thickness. The equations that define these parameters are well known (Ref. 10).

Optimization of the emitter and base regions was performed using PC-1D, a solar cell modeling program that solves the current continuity equation in one dimension. Recombination velocities at both AlGaAs/GaAs interfaces were held constant at 10^4 cm/s. The results for the optimized ultra-thin GaAs solar cell structure were similar to typical AlGaAs/GaAs heterostructure space solar cells, with the exception of a slight increase of the carrier concentration of the base layer, due to the optical confinement of the thin, light trapped structure. The optimized p-n characteristics for the thin, light-trapped GaAs solar cell are listed in Table 6.

TABLE 6. Optimized emitter and base region parameters.

Layer	thickness (μm)	carrier concentration (cm^{-3})
emitter (p)	0.3 - 0.5	$1\text{-}5x10^{18}$
base (n)	1	$5x10^{17}$

After establishing the optimum emitter and base region parameters, a three dimensional analysis was performed to minimize the resistive losses of the solar cell. Series resistance losses occur because of I^2R (Joule heating) losses in the conducting material. These losses are generally minimized by applying sufficient metallization to the front and back surface of the solar cell. A trade off exists between minimizing series resistance and decreasing the short circuit current due to the shading of sunlight by the front metallization.

The relevant losses to be calculated in the analysis are the contact shading loss and the Joule heating loss. The predicted output power from the solar cell is thus the optimized power calculated from the ideal diode model minus the sum of the transparency and resistive losses:

$$P_{out} = (P_{optimum})(transparency) - I^2 R$$

where the transparency is the ratio of active area to total area of the solar cell and the I^2R losses are determined by the volume integral

$$\iiint \rho J dx dy dz .$$

The above integral is taken over each of the individual regions and can be expressed analytically by the equations presented below. The symbols are defined in Table 7.

Emitter loss (including $Al_{.85}Ga_{.15}As$ window):

$$\frac{(\text{Im}\,T)^2 \rho W}{12Ltg^2}$$

Base loss (including $Al_{.85}Ga_{.15}As$ passivation):

$$\frac{(\text{Im}\,T)^2 \rho A}{LW}$$

Grid loss:

$$\frac{(\text{Im}\,T)^2 \rho L}{24n^2h^2gb^2}$$

Bus bar loss:

$$\frac{(\mathrm{Im}\,\mathrm{T})^2 \rho \mathrm{W}}{6\mathrm{Bm}^2\mathrm{h}^2}$$

TABLE 7. Parameter definitions for grid design calculations.

symbol	description
I_m	maximum current before correcting for transmission and reflectivity
T	transparency
t	emitter thickness
A	base thickness
ρ	resistivity of the corresponding layer
h	constant
m	bus bar dimension factor (mh = bus bar width)
n	grid width dimension factor
b	number of bus bars
g	number of grids
L	length of solar cell
W	width of solar cell

Based on the results of an Excel model, the optimum grid design consisted of one bus bar approximately 100 μm in width and ten grid lines approximately 30 μm in width. Processing yields were also considered for the final design. A contact pad approximately 0.005 cm^2 was incorporated to provide sufficient area for lead attachment. Total losses due to grid shading and series resistance were 5% for this design.

3.5 Task 5. Characterize the thin, light trapped GaAs solar cell.

<u>Gray I-V measurements</u>

Measuring the short circuit current and open-circuit voltage of a device under a wide range of light intensities (gray JV) provides a quantitative measurement of the leakage current due to generation-recombination in the depletion region. The light induced current is reduced by two reverse saturation (dark) diode currents, and by losses due to series and shunt resistance. Gray and dark JV measurements can be used to determine solar cell performance parameters such as R_{SERIES}, R_{SHUNT}, reverse saturation currents, and the diode ideality (n) factor at the operating point. The shape of the dark and gray JV curves is material and current dependent. At very low currents, the device behavior is dominated by the diode shunt resistance. As the current increases, the J_{02} space charge recombination current begins to dominate. At higher currents, the J_{01} diffusion current tends to be the dominating loss mechanism and as the current increases further, the series resistance of the device becomes the final dominating loss mechanism.

The loss mechanisms that can be characterized by this procedure are given by the last three terms on the right hand side of the following equation

$$J = J_L - \frac{V + JR_s}{R_{sh}} - J_{02}\left(e^{\frac{V+JR_s}{2V_T}} - 1\right) - J_{01}\left(e^{\frac{V+JR_s}{V_T}} - 1\right)$$

where the order of the loss mechanisms is essentially the same as that which can be determined from the experimental data. If a device is dominated by resistance effects, the reverse saturation currents cannot usually be determined. An approximate value of R_{SHUNT} can be obtained from these data by applying Ohm's law to several gray JV points measured under low illumination levels.

For J_{01}, the theoretical values are known as a function of temperature and bandgap (Ref. 11). This is given by

$$J_{01} = CT^3 e^{\frac{-E_g}{2kT}} \quad C = 660 \mu A/cm^2K^3$$

An approximation of the theoretical value of J_{02} is given by taking the square root of J_{01} in the above equation.

Both J_{01} and J_{02} may be found using a graphical technique. The line representing J_{02} vs. voltage data has an inverse slope of 0.120 V/decade on a semi-log scale at room temperature. The line can be superimposed on the data line at a point where there is a similar slope. The y-intercept of this line is J_{02}. The J_{01} current may be found in a similar manner. The J_{01} line has an inverse slope of 0.06 V/decade. If it is superimposed on the data curve at a point of equal curvature, its y-intercept is J_{01}. Figure 17 illustrates a high leakage GaAs solar cell compared to one with good shunt resistance. The curvature of solar cell G13901E corresponds to the shunt resistance (5 MΩ-cm^2) of that device.

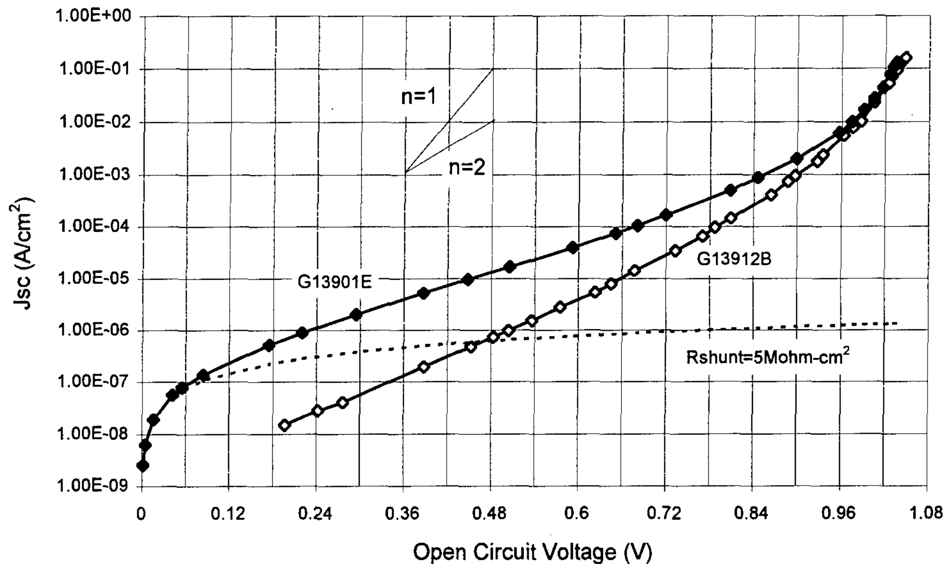

FIGURE 17. Gray JV data for a high leakage and low leakage GaAs solar cell.

Solar cell G13912B has a $J_{01}= 3.5x10^{-19}$ A/cm^2, $J_{02}=3x10^{-11}$ A/cm^2, and a specific shunt resistance > 10^7 Ω-cm^2. The shunt resistance of the electrometer used to make these measurements is 10^{14} Ω. This solar cell was sent to Phillips Laboratory as a hardware deliverable. The AM0, 1X efficiency was 17.6% (see Section 3.6.1).

Table 8 lists the leakage current values of some of the GaAs solar cells fabricated during the Phase II program. The dark diode current values obtained at AstroPower are among the best reported by a number of researchers for high efficiency heteroface GaAs solar cells (Refs. 12-14).

TABLE 8. Leakage currents of some of the GaAs solar cells measured during the Phase II program.

Device	V_{oc} (volts)	J_{sc} (mA/cm^2)	FF (%)	Efficiency (%)	J_{01} (A/cm^2)	J_{02} (A/cm^2)
G13901A	1.013	29.8	80.5	17.9	$5x10^{-19}$	$8x10^{-10}$
G13901B	1.015	30.0	79.3	17.9	$5x10^{-19}$	$9x10^{-11}$
G13912B	1.012	23.4 (no AR)	82.3	14.4 (no AR)	$3x10^{-19}$	$5x10^{-11}$
G13912D	1.011	23.3 (no AR)	79.9	13.9 (no AR)	$3.5x10^{-19}$	$3x10^{-11}$
G13601C	1.005	28.5	77.8	16.5	$3x10^{-19}$	$5x10^{-11}$
G13604C	0.980	23.8 (no AR)	72.7	12.6 (no AR)	$4x10^{-19}$	$2x10^{-10}$
G13609C	0.997	24.2 (no AR)	73.1	13.1 (no AR)	$5x10^{-19}$	$9x10^{-11}$
G13609F	1.009	24.5 (no AR)	83.1	15.2 (no AR)	$4x10^{-19}$	$4x10^{-11}$
G13405D	1.014	28.3	82.0	17.4	$5x10^{-19}$	$1x10^{-10}$

In addition to the gray JV measurements, device performance potential was also determined by spectral response measurements and by measuring the current-voltage characteristics of the ultra-thin, light trapped GaAs solar cells. Results of these measurements for some of the devices fabricated during the Phase II program are included in Section 3.6, Task 6. The results for the ten best effort hardware deliverables are also included in this section.

3.6 Task 6. Sample and Device Fabrication.

The results of six 1 cm^2 devices processed from one 2x4 cm^2 LPE growth are shown in Table 9. The performance of these devices demonstrates the capability of the material to support large area devices.

TABLE 9. Current-voltage characteristics of six 1 cm^2 devices fabricated from one large area ($8cm^2$) LPE growth.

Cell Number	Voc (V)	Jsc (mA/cm^2)	Fill Factor (%)	Efficiency (AM0, 1X, 25°C) on GaAs substrate (%)	Efficiency (AM0, 1X, 25°C) of Ultra-thin Device (%)
G13901A	1.020	29.0	78.9	17.29	17.98
G13901B	1.015	30.0	79.3	17.89	17.56
G13901C	1.007	29.1	78.3	16.98	16.98
G13901D	1.008	30.2	73.8	16.64	13.94
G13901E	1.011	31.0	78.4	18.20	17.30
G13901F	0.987	30.8	72.5	16.33	15.17
Median	1.010	30.1	76.4	17.14	17.14

3.6.1 Fabrication of final prototype solar cell samples.

The final prototype solar cells were fabricated based on the results of the previously presented research. Results of the ten best effort deliverables are summarized in Table 10. The current-voltage curves and spectral response measurements for each of these devices is also presented. These results are a clear demonstration of the potential performance of the thin, light-trapped GaAs solar cell technology.

TABLE 10. Electrical Characteristics of ten best effort light-trapped, thin GaAs solar cells.

Sample Number	Open Circuit Voltage (V)	Short Circuit Current (mA)	Fill Factor (%)	AM0 Efficiency (%)
G13506D	1.014	28.91	78.9	17.1
G13601C	1.007	28.58	78.9	16.8
G13601E	1.011	29.22	77.9	17.0
G13901A	1.015	29.54	80.3	17.9
G13901C	1.006	29.46	76.4	16.7
G13901E	1.006	30.22	76.0	17.1
G13905F	0.980	25.90	79.2	14.9
G13906A	0.982	26.88	78.2	15.3
G13912A	0.992	30.27	65.0	14.4
G13912B	1.007	29.58	79.4	17.6

The current-voltage curves and external quantum efficiency curves for each of the ten best effort deliverables sent to Phillips Laboratory are shown on the following pages.

sample	G13506D
Voc	1.014 V
Jsc	28.91 mA/cm^2
Fill Factor	78.9%
Area	1 cm^2
Thickness	3 μm
AM0, 1X efficiency	17.1%

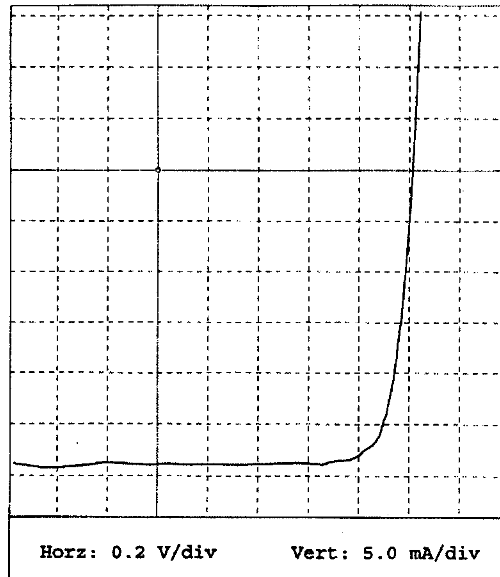

FIGURE 18. Current-voltage characteristics for deliverable G13506D.

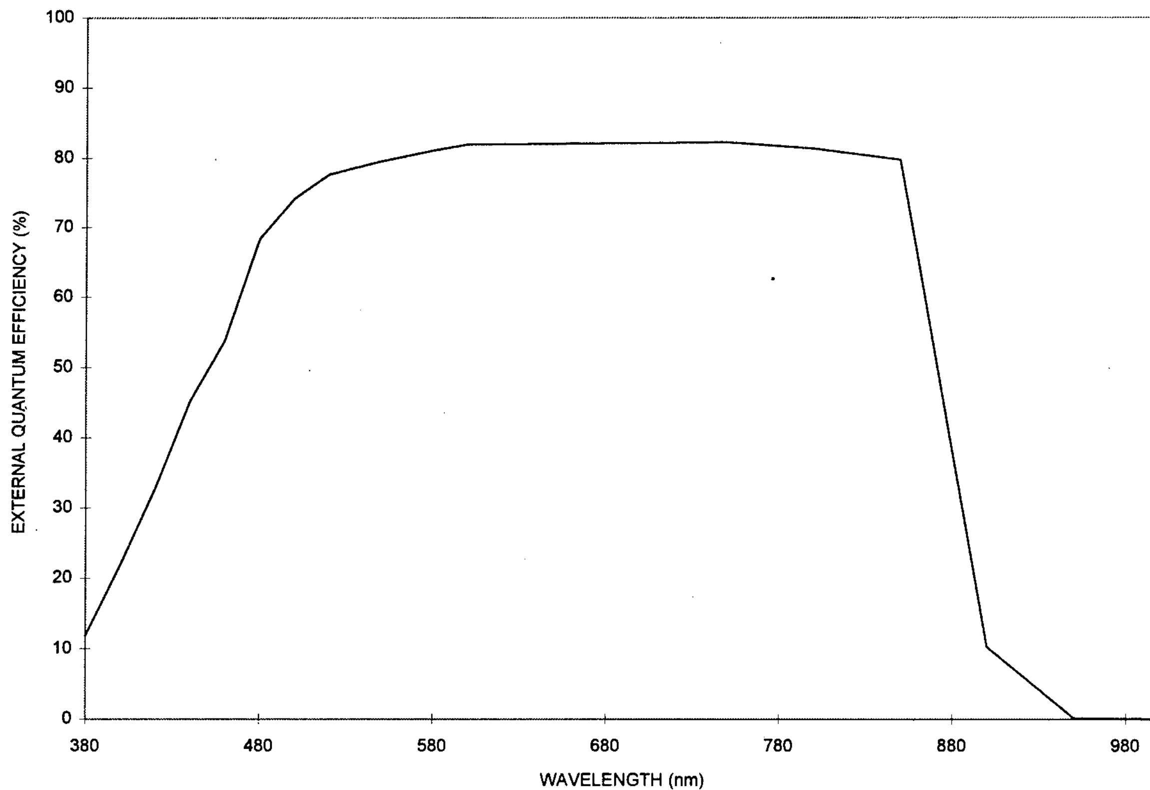

FIGURE 19. External quantum efficiency of deliverable G13506D.

sample	G13601C
Voc	1.007 V
Jsc	28.58 mA/cm^2
Fill Factor	78.9%
Area	1 cm^2
Thickness	3 μm
AM0, 1X efficiency	16.8%

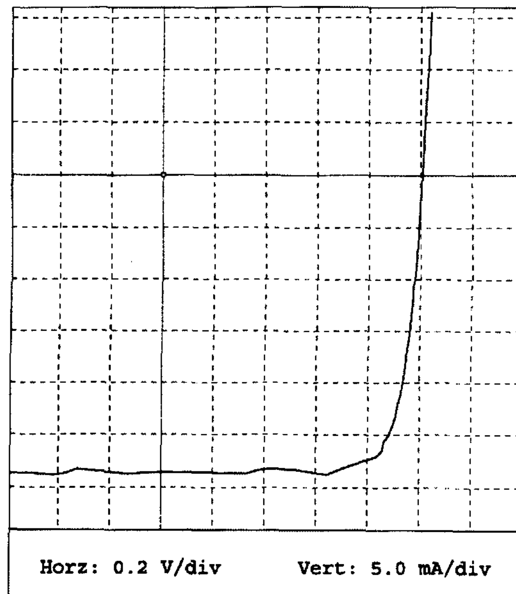

FIGURE 20. Current-voltage characteristics for deliverable G13601C.

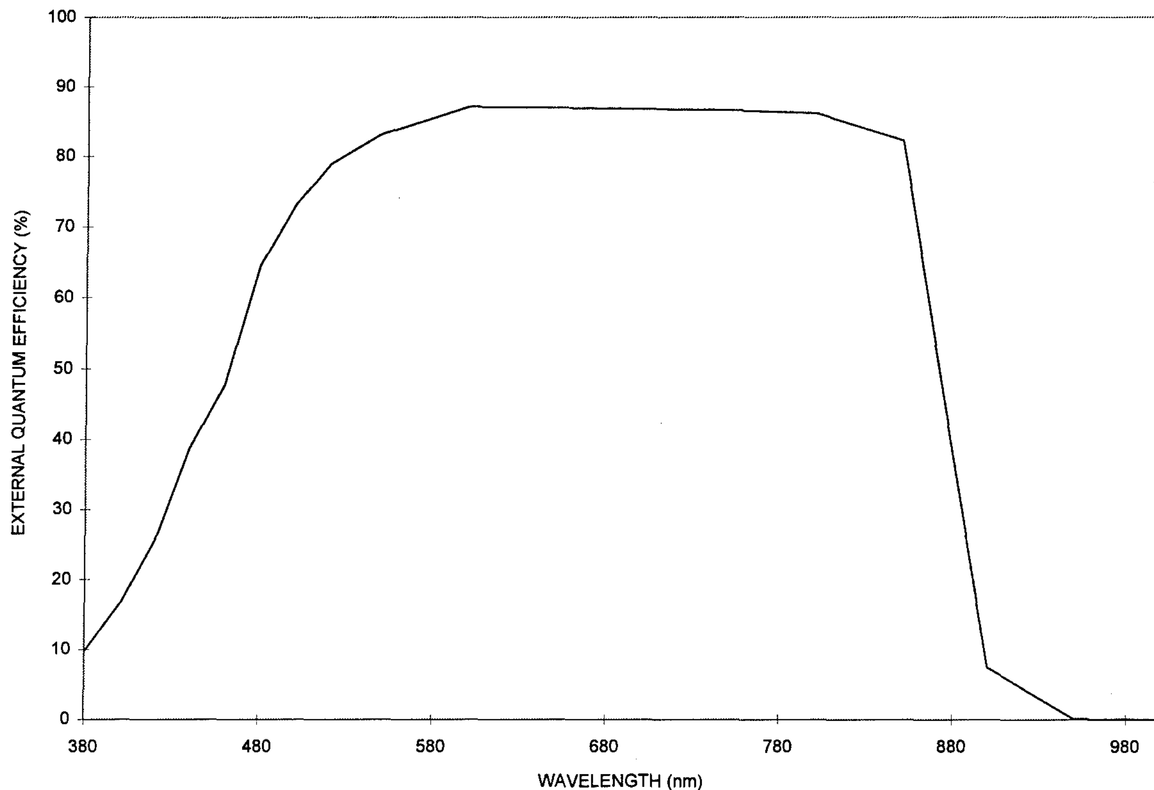

FIGURE 21. External quantum efficiency for deliverable G13601C.

sample	G13601E
Voc	1.011 V
Jsc	29.22 mA/cm^2
Fill Factor	77.9%
Area	1 cm^2
Thickness	3 μm
AM0, 1X efficiency	17.0%

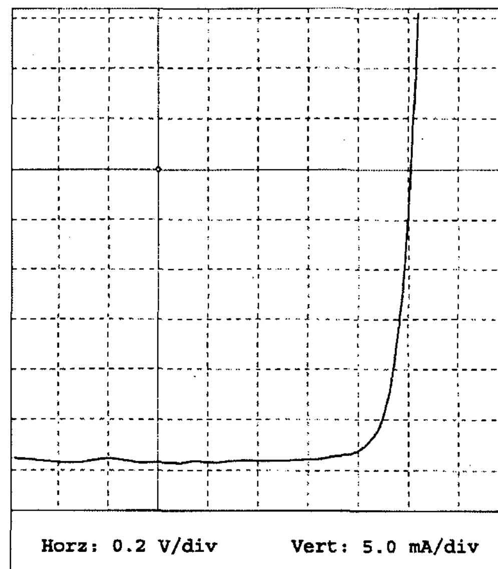

FIGURE 22. Current-voltage characteristics for deliverable G13601E.

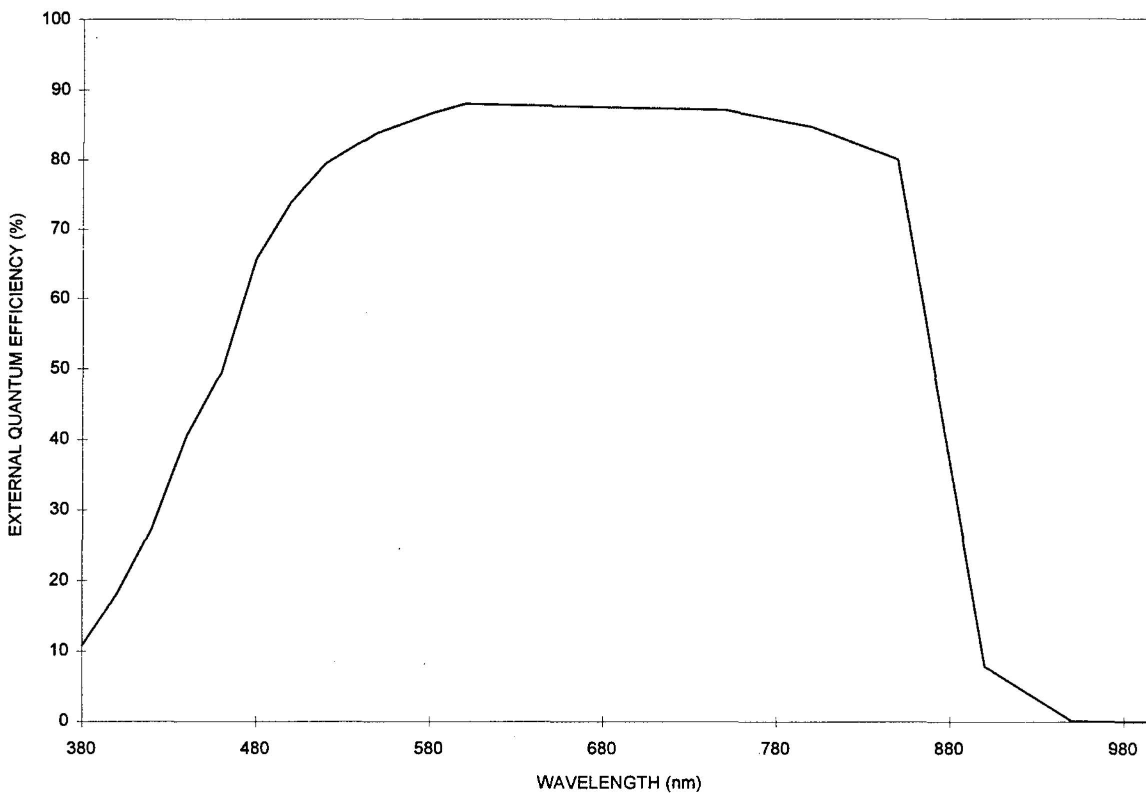

FIGURE 23. External quantum efficiency curve for deliverable G13601E.

sample	G13901A
Voc	1.015 V
Jsc	29.54 mA/cm^2
Fill Factor	80.3%
Area	1 cm^2
Thickness	3 μm
AM0, 1X efficiency	17.9%

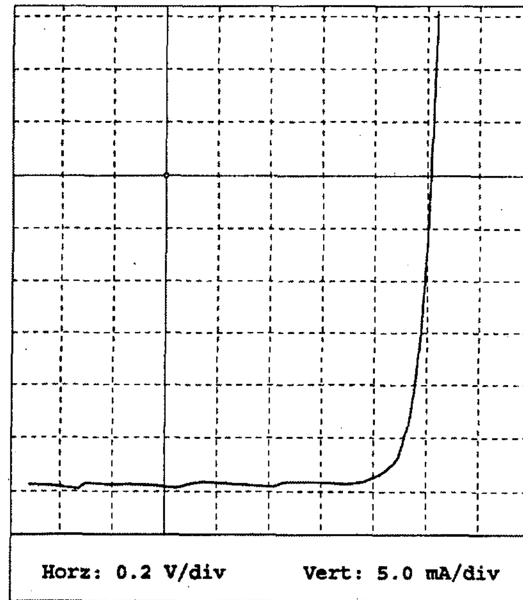

FIGURE 24. Current-voltage characteristics for deliverable G13901A.

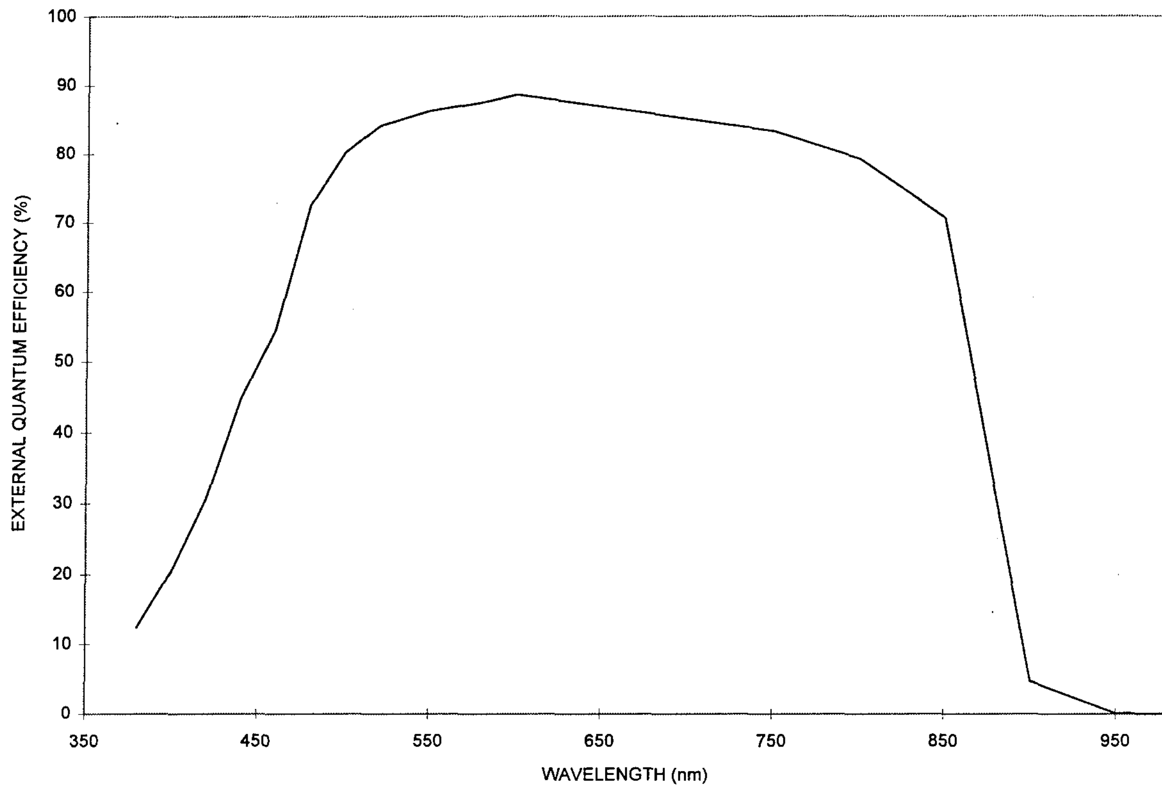

FIGURE 25. External quantum efficiency for deliverable G13901A.

sample	G13901C
Voc	1.006 V
Jsc	29.46 mA/cm^2
Fill Factor	76.4%
Area	1 cm^2
Thickness	3 μm
AM0, 1X efficiency	16.7%

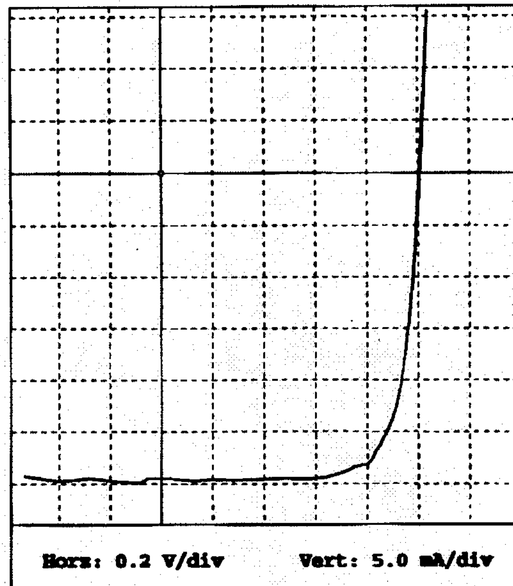

FIGURE 26. Current-voltage characteristics for deliverable G13901C.

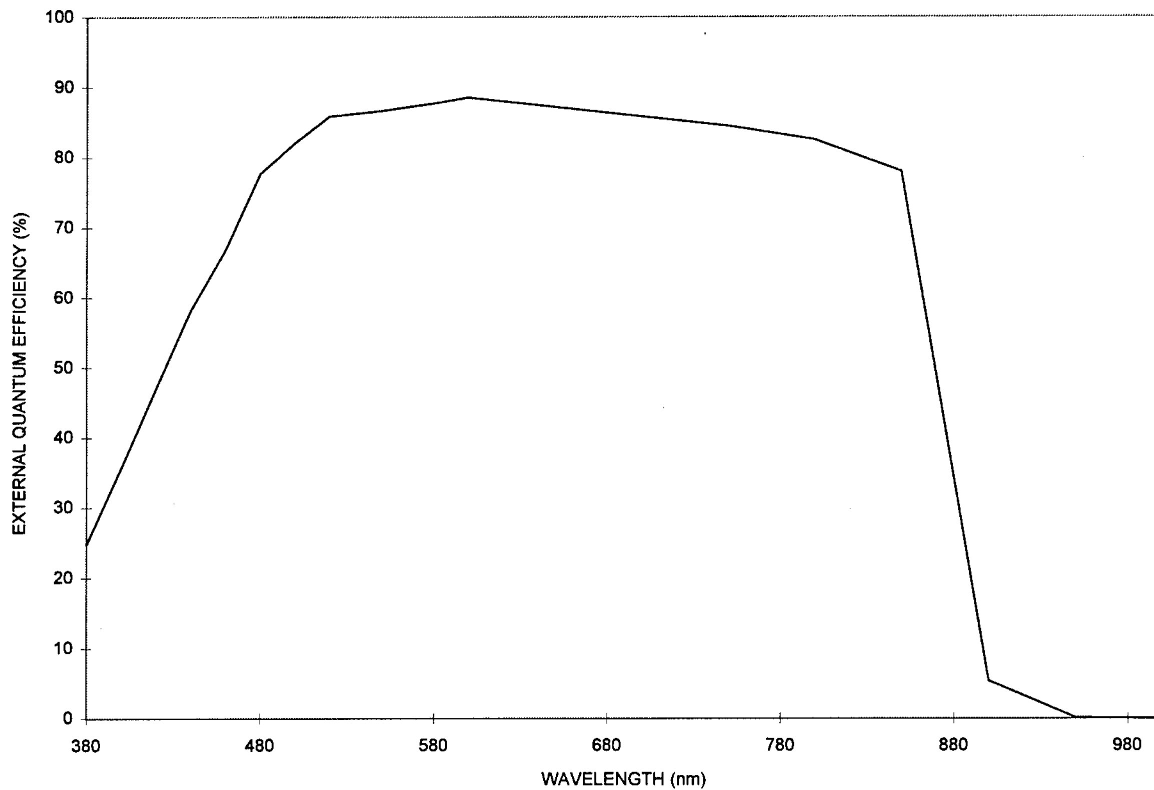

FIGURE 27. External quantum efficiency for deliverable G13901C.

sample	G13901E
Voc	1.006 V
Jsc	30.22 mA/cm^2
Fill Factor	76.0%
Area	1 cm^2
Thickness	3 μm
AM0, 1X efficiency	17.1%

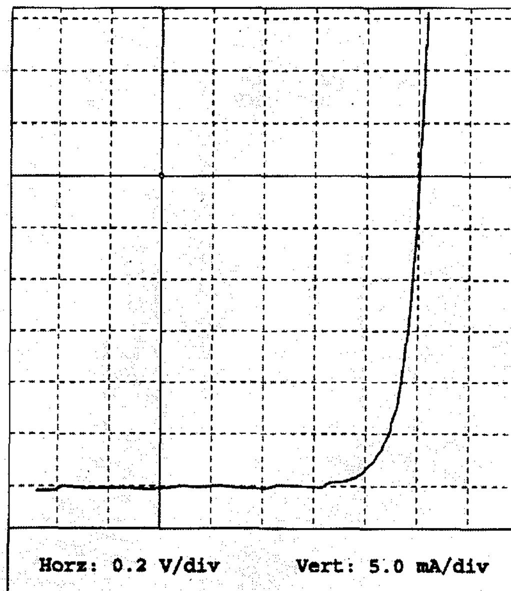

FIGURE 28. Current-voltage characteristics for deliverable G13901E.

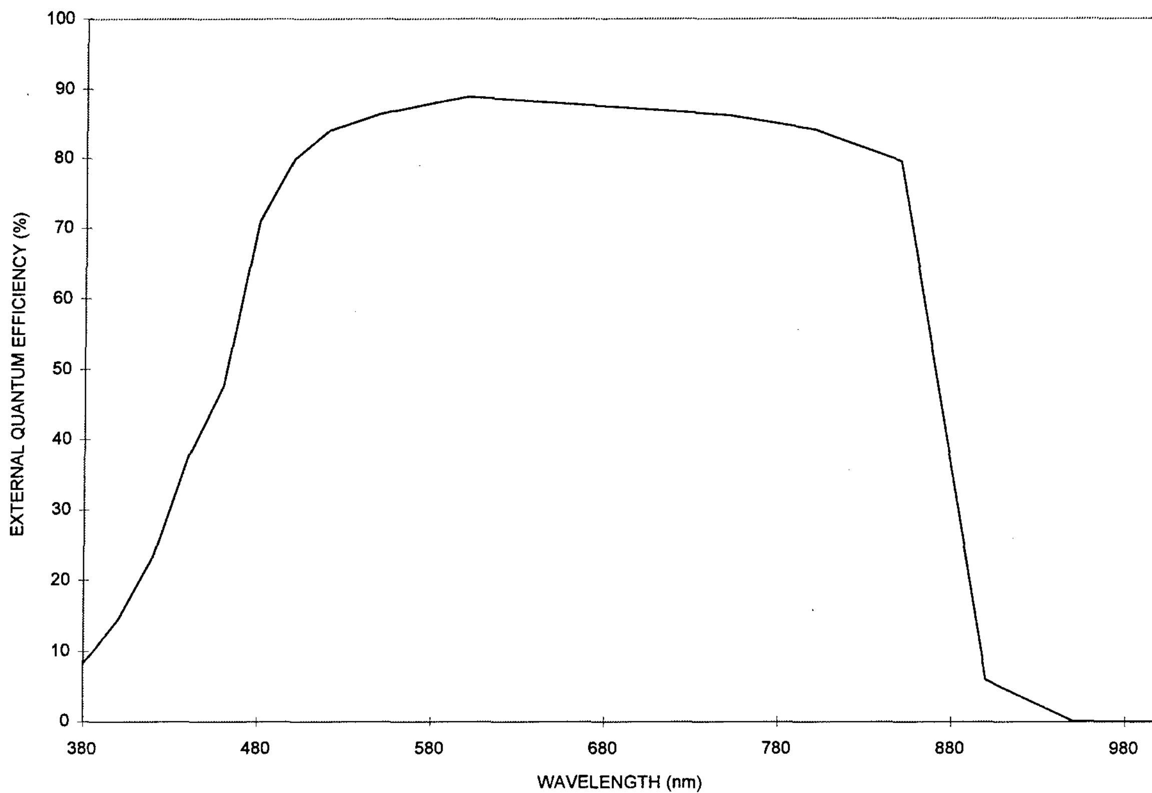

FIGURE 29. External quantum efficiency for deliverable G13901E.

sample	G13905F
Voc	0.980 V
Jsc	25.90 mA/cm^2
Fill Factor	79.2%
Area	1 cm^2
Thickness	3 μm
AM0, 1X efficiency	14.9%

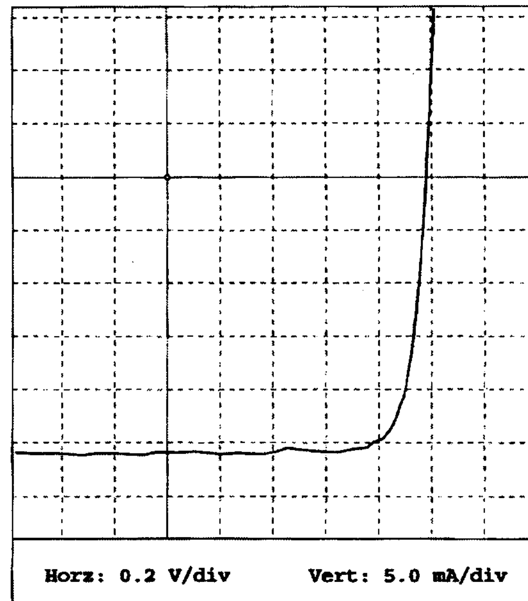

FIGURE 30. Current-voltage characteristics for deliverable G13905F.

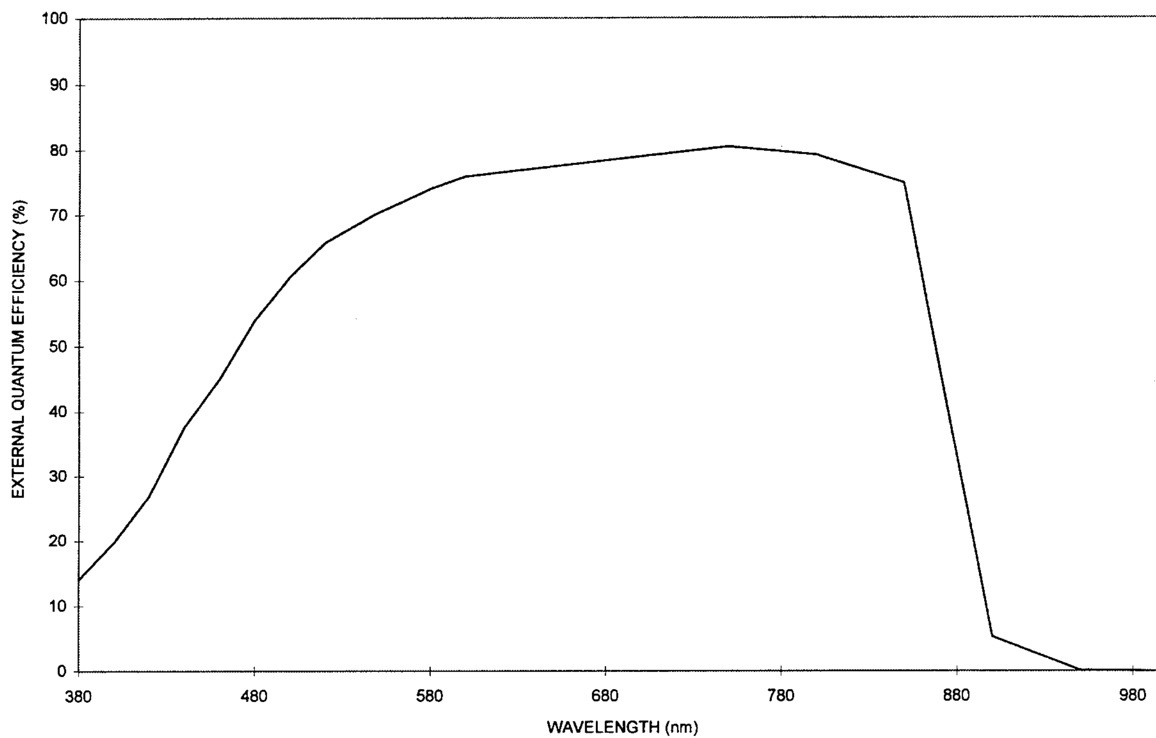

FIGURE 31. External quantum efficiency for deliverable G13905F.

sample	G13906A
Voc	0.982 V
Jsc	26.88 mA/cm^2
Fill Factor	78.2%
Area	1 cm^2
Thickness	3 μm
AM0, 1X efficiency	15.3%

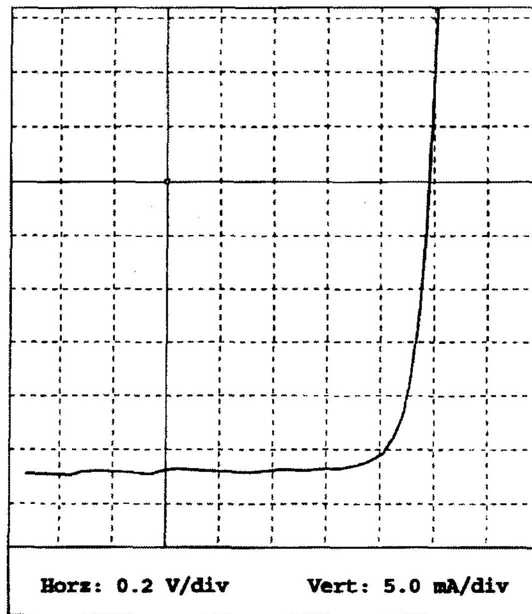

FIGURE 32. Current-voltage characteristics for deliverable G13906A.

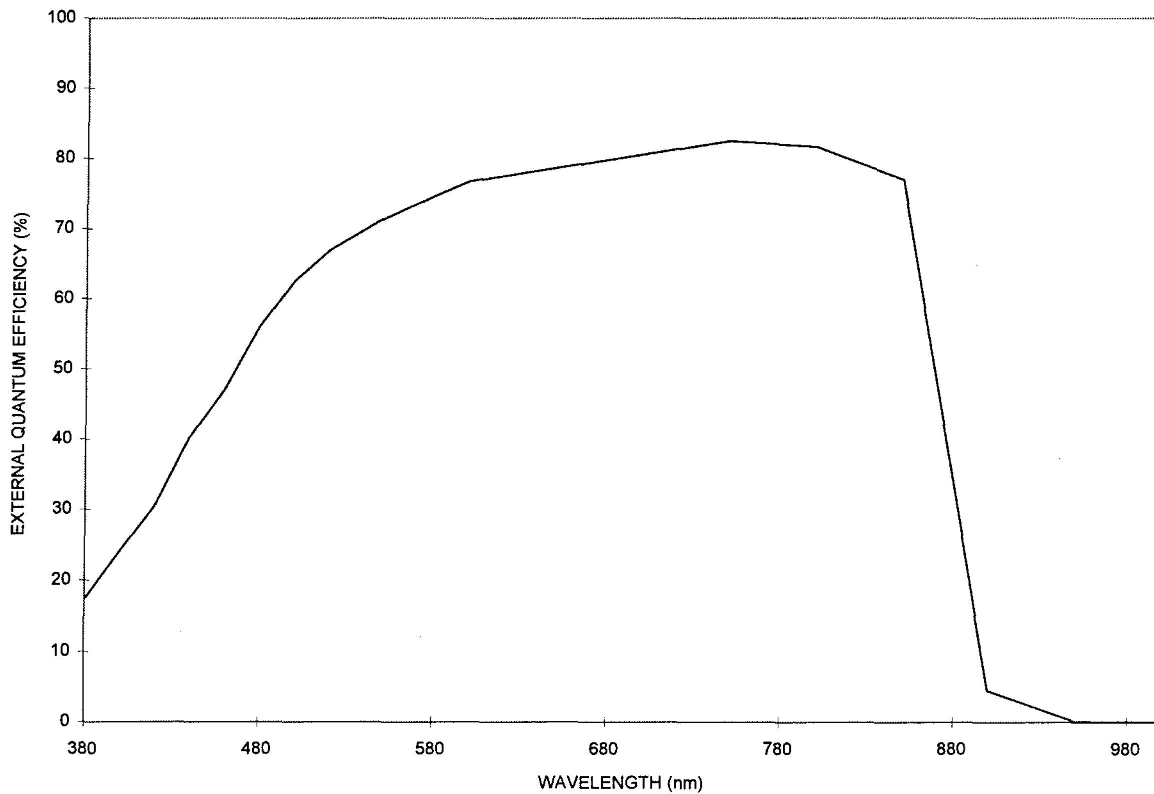

FIGURE 33. External quantum efficiency for deliverable G13906A.

sample	G13912A
Voc	0.992 V
Jsc	30.27 mA/cm^2
Fill Factor	65.0%
Area	1 cm^2
Thickness	3 μm
AM0, 1X efficiency	14.4%

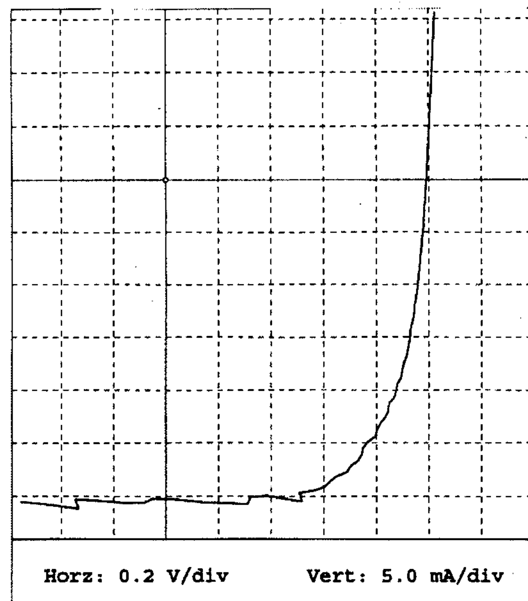

FIGURE 34. Current-voltage characteristics for deliverable G13912A.

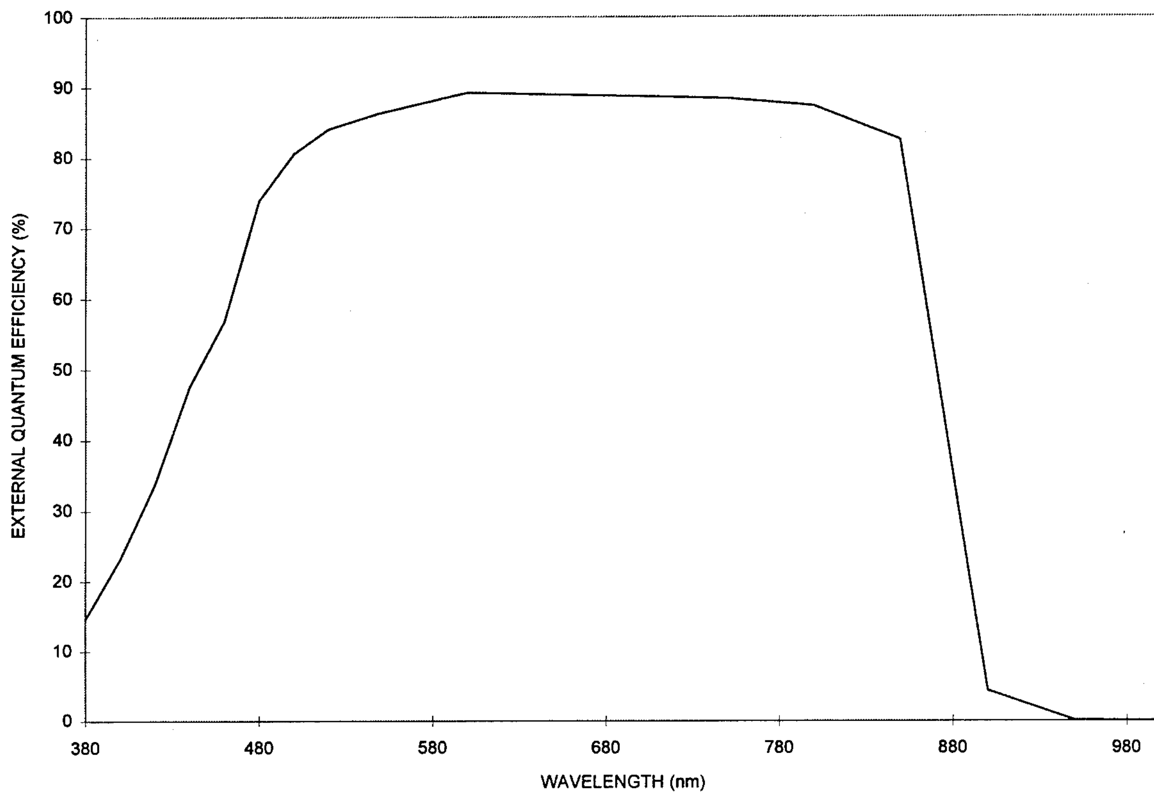

FIGURE 35. External quantum efficiency for deliverable G13912A.

sample	G13912B
Voc	1.007 V
Jsc	29.58 mA/cm^2
Fill Factor	79.4%
Area	1 cm^2
Thickness	3 μm
AM0, 1X efficiency	17.6%

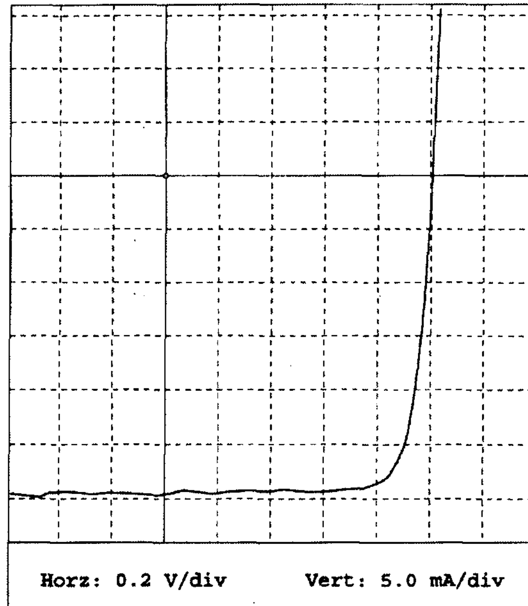

FIGURE 36. Current-voltage characteristics for deliverable G13912B.

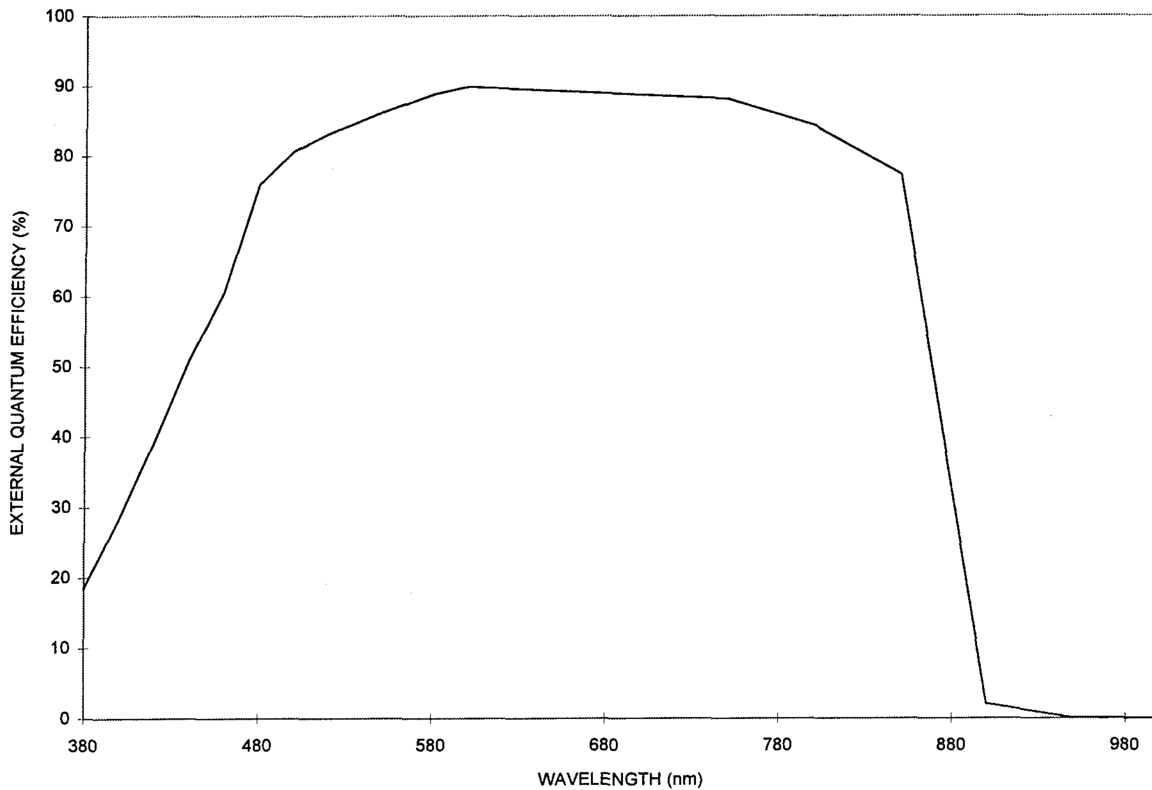

FIGURE 37. External quantum efficiency curve for deliverable G13912B.

3.7 Task 7. Thermal Cycle Testing.

Thermal stress testing experiments were conducted for two thin, light-trapped GaAs solar cells. The samples received 100 cycles from -80°C to +120°C. The cycle time was approximately 10 minutes. The thermal cycling system uses forced convection with liquid nitrogen as the coolant and a serpentine array as the heat source. No attempt was made to control the gas ambient inside this unit.

The device performance was monitored after 8, 25, 29 and 38 cycles for a total of 100 cycles. Standard I-V curves were measured from which the open circuit voltage, short circuit current, fill factor, and efficiency were obtained. As indicated in Table 11, there was no degradation to the device performance after the thermal cycling, and there was no loss of structural integrity or change in physical appearance. Any change in the output parameters is due to experimental error of the efficiency measurement.

TABLE 11. Comparison of solar cell electrical performance before and after 100 thermal cycles.

cell #	Voc (0) volts	Voc (100) volts	Jsc (0) mA/cm^2	Jsc (100) mA/cm^2	FF (0) %	FF (100) %	η (0) %	η (100) %
G13504D	1.005	1.006	26.50	27.35	72.0	72.4	14.2	14.8
G13906B	0.975	0.975	26.37	26.43	75.3	76.1	14.3	14.5

In addition to the thermal cycle data, the current-voltage characteristics of a GaAs solar cell were measured at elevated temperatures. These measurements were completed with the thin GaAs solar cell structure on the GaAs substrate. The data for open circuit voltage, short circuit current, fill factor and efficiency as a function of temperature are shown in Figure 38. This structure was not optimized for elevated temperatures. The Au/Zn/Au metal system makes direct contact to the p-type emitter. Including a front surface, GaAs, p-type contact layer may further enchance the high temperature capabilities of the GaAs solar cell.

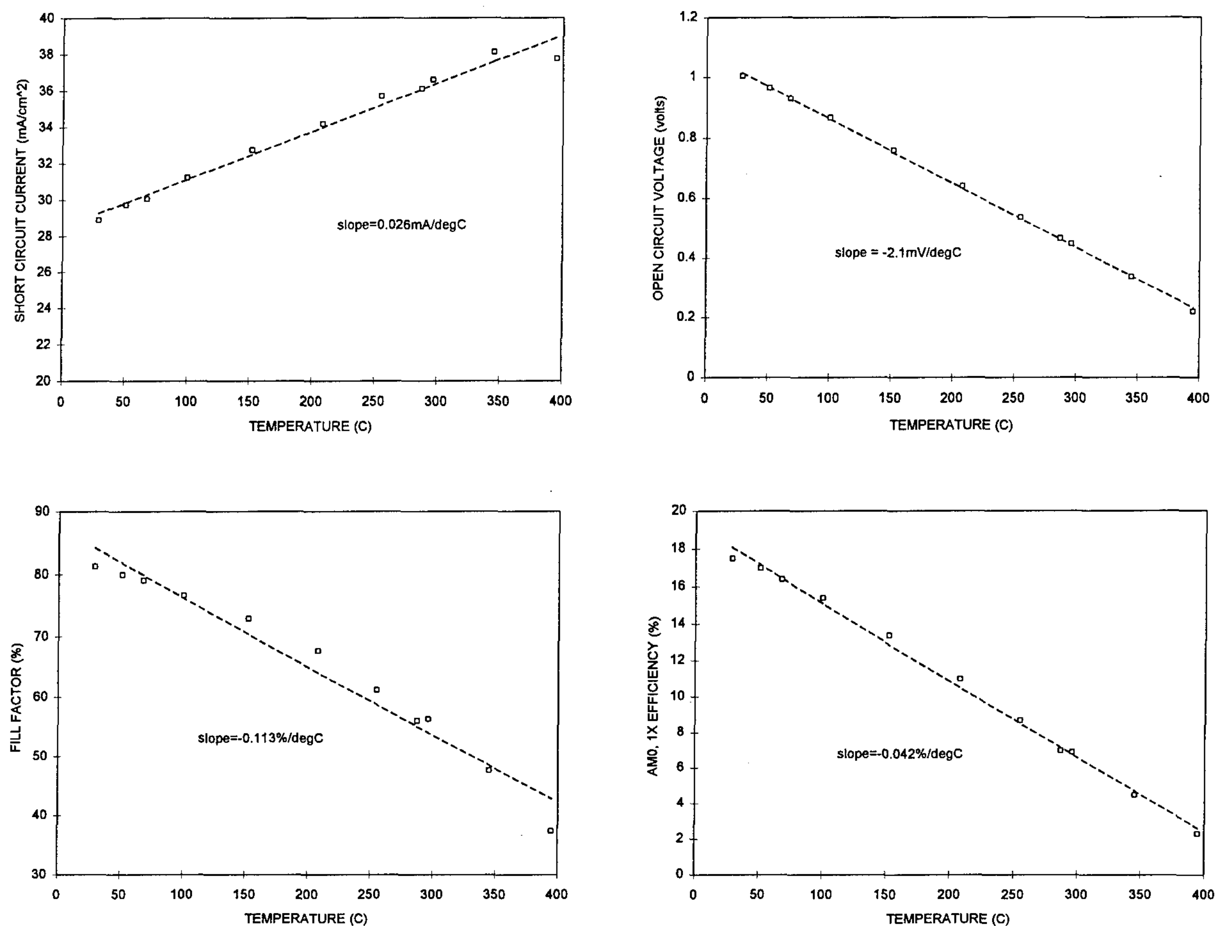

FIGURE 38. High temperature current-voltage characteristics of GaAs solar cell G14002.

3.8 Task 8. Manufacturing feasibility study.

Liquid phase epitaxy was used in this program. Materials grown by LPE have consistently shown electronic properties superior to those of materials grown by other techniques. In fact, most materials grown by MOCVD and MBE are compared to those grown by LPE to determine the impact of improvements gained in the growth process. Liquid phase epitaxy has continually demonstrated superior material in terms of diffusion length, lifetime, and deep level impurities. In addition to these inherent features, the growth of GaAs via the liquid phase has demonstrated superior material at growth rates sufficient to fabricate high quality GaAs in production quantities.

LPE is low cost compared to alternative fabrication technologies such as MOCVD because of its high productivity in each cost component: material, labor, and capital. In the following discussion we will describe the fundamental cost limitations of LPE and MOCVD,

indicate the advantages of LPE compared to MOCVD, and finally give a detailed cost estimate of the GaAs solar cell.

Material Cost - Substrates

GaAs substrates for the thin GaAs solar cell have to be removed to allow the benefits of thin solar cell designs to be utilized and offer a very lightweight and high specific power product. This is normally a very expensive proposition because of the sacrifice of the expensive starting GaAs material itself. For example, 4-cm x 4-cm substrates suitable for GaAs solar cells would cost in the range of $69-$91 in production quantities. This starting material cost has led a number of researchers to propose various elegant and/or remarkable techniques for removing the active GaAs layer and re-using the expensive substrate. These processes have not been demonstrated for large area or at high yield. Our experience has shown that LPE growth of GaAs is relatively tolerant to substrate quality. As a result, the natural improvement in quality of the grown layer, which is realized by LPE, can be used to advantage. It may be possible to use substrates of low quality and still grow a high quality solar cell or utilize GaAs on germanium technology to reduce this cost. The substrate will then be removed by etching and thus be discarded. At the present time and in this study we have not utilized this approach and it is not included in the cost analysis in order to present the manufacturing costs in a near term scenario.

Materials Cost - Processing

Initially, the information gathered from this Phase II program was used to develop the actual cost of prototype devices disregarding the actual research and development cost itself. Based on the average labor cost, present materials costs, throughput, prototype process, and solar cell size and efficiency, a prototype device cost was generated.

Following the determination of the prototype cost, a survey of existing facilities and capabilities was undertaken to estimate the possible throughput of the GaAs facility. With this information, throughput for a pilot production effort of 400 wafer starts per month and a low volume production effort of 1000 wafer starts per month were projected. These numbers are phenomenally small when compared to the current production of silicon solar cells of 100,000 wafer starts per month, however, the market for GaAs solar cells is much smaller and would not support manufacturing at this level even though the cost of the final product would be drastically reduced. Obviously, if it were justifiable to manufacture at a level of 100,000 wafer starts per month, the cost of the GaAs solar cell would be at most only a few dollars more than the cost of the substrate and the epitaxial growth step.

Actual data derived from the Phase II program and vendor quotes at various levels of delivery yielded cost points for the projected solar cell costs. It should be noted that the GaAs substrates are based on 8-cm^2 wafers for the prototype solar cell and progress to 3-inch wafers for the pilot production and production cost estimates. Table 12 is a summary of the three cases that were examined. The fully loaded costs shown in the table encompass projected yield, overhead, and general and administrative costs.

TABLE 12. Projected solar cell costs.

Wafer Cost	Cells/Wafer	Cell Size (cm^2)	Labor Cost ($/hr.)	Efficiency	Cost/cm^2	Cost/Watt
Fully Loaded Prototype Solar Cell Cost						
53	6	1	$15.73	18%	$167.23	$6881.76
Fully Loaded Pilot Production Solar Cell Cost						
74	1	25	$12.00	20%	$15.03	$556.50
Fully Loaded Production Solar Cell Cost						
69	1	25	$10.00	22%	$12.36	$416.31

In the following pages are the details of the fabrication processes, direct materials costs, direct labor costs, and yield. Also included are the cumulative yields and the impact of the yield on the total cost of the solar cell. When moving from prototype to production it is assumed that the cost of labor will decrease and that the yield and quality of the product will increase. These assumptions are emphasized in the summary table and in the detailed projections.

Fully Loaded Prototype Production Cost

PROCESS	MATLS Direct Matls [$/wfr]	LABOR Set-Up Time [op-hr]	Process Rate [wfr/op-hr]	Effective Rate [wfr/op-hr]	Direct Labor [$/wfr]	YIELD ANALYSIS Yield	Good SC Cost [$/wfr]	Yield Cost [$/wfr]	Cumm Cost [$/wfr]
LPE Growth	82.86	3.00	0.33	0.21	76.27	0.75	212.17	53.04	212.17
FC Photolith									
[Surface Prep]	0.69	0.08	6.00	5.94	2.65	1.00	3.34	0.00	215.51
[Spray & Bake]	1.53	0.08	6.00	5.94	2.65	1.00	4.18	0.00	219.69
[Expose]	0.31	0.08	6.00	5.94	2.65	0.98	3.02	0.06	222.70
[Develop]	0.40	0.17	6.00	5.88	2.68	0.98	3.14	0.06	225.84
FC Evap	15.70	2.00	6.00	4.50	3.50	0.95	20.21	1.01	246.05
Metal Lift-Off	0.03	0.50	12.00	11.25	1.40	0.95	1.50	0.08	247.55
FC Plating Photolith									
[Spray & Bake]	0.01	0.08	6.00	5.94	2.65	0.95	2.80	0.14	250.35
[Expose]	0.40	0.08	6.00	5.94	2.65	0.95	3.21	0.16	253.56
[Develop]	0.40	0.17	6.00	5.88	2.68	0.95	3.24	0.16	256.80
Au Plating	0.19	2.00	3.00	2.25	6.99	0.85	8.45	1.27	265.25
[Spray & Bake]	0.01	0.08	6.00	5.94	2.65	0.95	2.80	0.14	259.60
Isolation	0.96	2.00	3.00	2.25	6.99	1.00	7.96	0.01	273.21
FC Tabbing	7.80	1.00	6.00	5.25	3.00	0.90	12.00	1.20	285.20
AR Coating	0.00	1.00	6.00	5.25	3.00	1.00	3.02	0.02	288.22
Glass Bonding	1.80	1.00	6.00	5.25	3.00	0.95	5.05	0.25	293.27
Thinning	3.41	2.00	2.00	1.50	10.49	0.90	15.44	1.54	308.71
BC Photolith									
[Surface Prep]	0.69	0.08	6.00	5.94	2.65	1.00	3.34	0.00	312.05
[Spray & Bake]	1.53	0.08	6.00	5.94	2.65	1.00	4.18	0.00	316.22
[Expose]	0.31	0.08	6.00	5.94	2.65	0.98	3.02	0.06	319.24
[Develop]	0.80	0.17	6.00	5.88	2.68	0.98	3.55	0.07	322.79
BC Evap	18.23	1.00	30.00	26.25	0.60	1.00	18.92	0.09	341.71
Metal Lift-Off	0.03	0.50	20.00	18.75	0.84	1.00	0.87	0.00	342.58
Reflector									
[Surface Prep]	0.69	0.08	6.00	5.94	2.65	1.00	3.34	0.00	345.92
[Spray & Bake]	1.53	0.08	6.00	5.94	2.65	1.00	4.18	0.00	350.10
[Expose]	0.31	0.08	4.00	3.96	3.97	0.98	4.37	0.09	354.47
[Develop]	0.80	0.17	6.00	5.88	2.68	0.98	3.55	0.07	358.02
[Reflector Evap]	2.00	1.00	30.00	26.25	0.60	1.00	2.61	0.01	360.63
Anneal	0.00	0.17	20.00	19.58	0.80	0.80	1.01	0.20	361.64
Test/Inspct	0.02	1.00	6.00	5.25	3.00	0.90	3.35	0.33	364.99
TOTAL	**$143.45**				**$164.27**		**$367.79**	**$60.07**	**$364.99**

Fully Loaded Pilot Production

PROCESS	MATLS Direct Matls [$/wfr]	LABOR Set-Up Time [op-hr]	Process Rate [wfr/op-hr]	Effective Rate [wfr/op-hr]	Direct Labor [$/wfr]	YIELD ANALYSIS Yield	Good SC Cost [$/wfr]	Yield Cost [$/wfr]	Cumm Cost [$/wfr]
LPE Growth	103.86	3.00	2.00	1.25	9.60	0.90	126.07	12.61	126.07
FC Photolith									
[Surface Prep]	0.69	0.08	12.00	11.88	1.01	1.00	1.70	0.00	127.77
[Spray & Bake]	1.53	0.08	30.00	29.70	0.40	1.00	1.93	0.00	129.70
[Expose]	0.31	0.08	30.00	29.70	0.40	0.98	0.73	0.01	130.43
[Develop]	0.40	0.17	30.00	29.38	0.41	0.98	0.83	0.02	131.25
FC Evap	15.70	2.00	30.00	22.50	0.53	0.95	17.09	0.85	148.34
Metal Lift-Off	0.03	0.50	30.00	28.13	0.43	0.95	0.48	0.02	148.82
FC Plating Photolith									
[Spray & Bake]	0.01	0.08	30.00	29.70	0.40	0.95	0.44	0.02	149.26
[Expose]	0.40	0.08	15.00	14.85	0.81	0.95	1.27	0.06	150.53
[Develop]	0.40	0.17	30.00	29.38	0.41	0.95	0.85	0.04	151.38
Au Plating	0.19	2.00	30.00	22.50	0.53	0.85	0.85	0.13	152.23
[Spray & Bake]	0.01	0.08	30.00	29.70	0.40	0.95	0.44	0.02	151.82
Isolation	0.96	2.00	20.00	15.00	0.80	1.00	1.76	0.00	153.99
FC Tabbing	1.30	1.00	30.00	26.25	0.46	0.90	1.95	0.20	155.95
AR Coating	0.00	1.00	90.00	78.75	0.15	1.00	0.16	0.00	156.10
Glass Bonding	7.50	1.00	20.00	17.50	0.69	0.95	8.62	0.43	164.72
Thinning	3.41	2.00	10.00	7.50	1.60	0.90	5.57	0.56	170.29
BC Photolith									
[Surface Prep]	0.69	0.08	30.00	29.70	0.40	1.00	1.09	0.00	171.38
[Spray & Bake]	1.53	0.08	15.00	14.85	0.81	1.00	2.34	0.00	173.72
[Expose]	0.31	0.08	30.00	29.70	0.40	0.98	0.73	0.01	174.45
[Develop]	0.80	0.17	30.00	29.38	0.41	0.98	1.23	0.02	175.68
BC Evap	18.23	1.00	30.00	26.25	0.46	1.00	18.78	0.09	194.46
Metal Lift-Off	0.03	0.50	20.00	18.75	0.64	1.00	0.67	0.00	195.13
Reflector									
[Surface Prep]	0.69	0.08	30.00	29.70	0.40	1.00	1.09	0.00	196.23
[Spray & Bake]	1.53	0.08	30.00	29.70	0.40	1.00	1.93	0.00	198.16
[Expose]	0.31	0.08	15.00	14.85	0.81	0.98	1.14	0.02	199.30
[Develop]	0.80	0.17	30.00	29.38	0.41	0.98	1.23	0.02	200.53
[Reflector Evap]	2.00	1.00	30.00	26.25	0.46	1.00	2.47	0.01	203.00
Anneal	0.00	0.17	20.00	19.58	0.61	0.80	0.77	0.15	203.78
Test/Inspct	0.02	1.00	30.00	26.25	0.46	0.90	0.53	0.05	204.30
TOTAL	**$163.65**				**$25.71**		**$204.74**	**$15.38**	**$204.30**

Fully Loaded Production Cost

PROCESS	MATLS Direct Matls [$/wfr]	LABOR Set-Up Time [op-hr]	Process Rate [wfr/op-hr]	Effective Rate [wfr/op-hr]	Direct Labor [$/wfr]	YIELD ANALYSIS Yield	Good SC Cost [$/wfr]	Yield Cost [$/wfr]	Cumm Cost [$/wfr]
LPE Growth	98.86	3.00	4.00	2.50	4.00	0.90	114.29	11.43	114.29
FC Photolith									
[Surface Prep]	0.69	0.08	24.00	23.76	0.42	1.00	1.11	0.00	115.40
[Spray & Bake]	1.53	0.08	60.00	59.40	0.17	1.00	1.70	0.00	117.10
[Expose]	0.31	0.08	60.00	59.40	0.17	0.98	0.49	0.01	117.59
[Develop]	0.40	0.17	60.00	58.75	0.17	0.98	0.58	0.01	118.17
FC Evap	15.70	2.00	60.00	45.00	0.22	0.95	16.76	0.84	134.93
Metal Lift-Off	0.03	0.50	60.00	56.25	0.18	0.95	0.22	0.01	135.15
FC Plating Photolith									
[Spray & Bake]	0.01	0.08	60.00	59.40	0.17	0.95	0.19	0.01	135.33
[Expose]	0.40	0.08	30.00	29.70	0.34	0.95	0.78	0.04	136.11
[Develop]	0.40	0.17	60.00	58.75	0.17	0.95	0.60	0.03	136.71
Au Plating	0.19	2.00	60.00	45.00	0.22	0.85	0.48	0.07	137.20
[Spray & Bake]	0.01	0.08	60.00	59.40	0.17	0.95	0.19	0.01	136.90
Isolation	0.96	2.00	40.00	30.00	0.33	1.00	1.29	0.00	138.49
FC Tabbing	1.30	1.00	60.00	52.50	0.19	0.90	1.66	0.17	140.15
AR Coating	0.00	1.00	180.00	157.50	0.06	1.00	0.07	0.00	140.21
Glass Bonding	7.50	1.00	40.00	35.00	0.29	0.95	8.20	0.41	148.41
Thinning	3.41	2.00	20.00	15.00	0.67	0.90	4.53	0.45	152.94
BC Photolith									
[Surface Prep]	0.69	0.08	60.00	59.40	0.17	1.00	0.86	0.00	153.80
[Spray & Bake]	1.53	0.08	30.00	29.70	0.34	1.00	1.87	0.00	155.66
[Expose]	0.31	0.08	60.00	59.40	0.17	0.98	0.49	0.01	156.15
[Develop]	0.80	0.17	60.00	58.75	0.17	0.98	0.99	0.02	157.14
BC Evap	18.23	1.00	60.00	52.50	0.19	1.00	18.51	0.09	175.66
Metal Lift-Off	0.03	0.50	40.00	37.50	0.27	1.00	0.30	0.00	175.95
Reflector									
[Surface Prep]	0.69	0.08	60.00	59.40	0.17	1.00	0.86	0.00	176.81
[Spray & Bake]	1.53	0.08	60.00	59.40	0.17	1.00	1.70	0.00	178.51
[Expose]	0.31	0.08	30.00	29.70	0.34	0.98	0.66	0.01	179.17
[Develop]	0.80	0.17	60.00	58.75	0.17	0.98	0.99	0.02	180.16
[Reflector Evap]	2.00	1.00	60.00	52.50	0.19	1.00	2.20	0.01	182.36
Anneal	0.00	0.17	40.00	39.17	0.26	0.80	0.32	0.06	182.68
Test/Inspct	0.02	1.00	60.00	52.50	0.19	0.90	0.23	0.02	182.92
TOTAL	**$158.65**				**$10.71**		**$183.10**	**$13.74**	**$182.92**

4. CONCLUSION

AstroPower has successfully completed the Phase II program by demonstrating the feasibility of the ultra-lightweight, thin, light trapped GaAs solar cell for advanced space power systems. Prototype devices were fabricated and tested with efficiencies as high as 17.9 % (AM0, 1X) for a 3 μm thick, 1 cm^2 solar cell. This results in a specific power of 1020 W/kg (with a 3-mil cover slide) and a power density of 240 W/m^2. This technology will result in a revolutionary improvement in survivability, performance, and manufacturability of lightweight GaAs solar cell products for future Earth-orbiting science and space exploration missions. At the present time, AstroPower is capable of producing these high performance devices in limited quantities and intends to commercialize the thin GaAs product.

5. RECOMMENDATIONS

A number of innovative technologies were discovered during the course of the Phase II SBIR program which should be further explored and developed to: 1) further improve the specific product, and 2) create new applications for the techniques. Two of the most significant discoveries are described in the following section and recommendations are made for future action.

Adhesive Bonding Technology

Various new adhesive bonding approaches need to be considered. In order to prove the potential of the thin GaAs solar cell, only a limited effort was executed to development of the solar cell to glass bonding. Alternative bonding agents as well as teflon films should be evaluated and developed. The bonding technology can enable significant new optoelectronic products involving multi-layer structures of the same or dissimilar materials, including such devices as multi-wavelength detector stacks, buried waveguides, buried reflectors, and the ability to monolithically assemble devices of dissimilar materials. This bonding technology, as opposed to direct glass bonding, will also enable transparent device designs that can be used for mechanical tandem stacks.

Plasma Annealed Contacts

This low temperature contact annealing technique is another innovation that can be applied to a broad range of devices and material systems. Reducing the temperature required to form ohmic contacts can have a significant impact on the quality of fabricated devices due to the lower induced stress on the material and device layers and reduction in migration of dopants and metals. The technique should be developed and a determination should be made if it is viable to design and manufacture production equipment to implement this technique in the commercial semiconductor sector.

In summary, the SBIR Phase II program demonstrated the potential of the thin GaAs solar cell and it is necessary to further develop manufacturing techniques and to implement pilot production. AstroPower is also capable, at this point, to deliver prototype thin GaAs solar cells for test and evaluation before committing to a full manufacturing effort.

6. REFERENCES

1. P Iles and F. Ho, “Technology Challenges for Space Solar Cells, Proc. 24th IEEE Photovoltaic Specialists Conference, (1994).

2. K. Gaffney, “Air Force Activities in Space Photovoltaic Power System Technology”, Proc. NASA Space Photovoltaic Research and Technology Conference, Cleveland, Ohio (1994).

3. C.B. Honsberg and A.M. Barnett, “Light trapping in Thin Film GaAs Solar Cells”, Proc. 22nd IEEE Photovoltaic Specialists Conference, Las Vegas, Nevada, (1991).

4. H. Nelson, RCA Review, 24 (1963) page 603.

5. M.E. Nell, D. Lin, H. Eschrich, and H.G. Wagemann, “Beryllium Diffusion for AlGaAs/GaAs Solar Cells by Single Melt LPE”, Ninth E.C. PVSEC, September, 1989, pg. 126.

6. L.J. Brillson, Contacts to Semiconductors, Noyes Publications, Park Ridge, New Jersey, 1993, pg. 382.

7. S.M. Sze, Physics of Semiconductor Devices, John Wiley & Sons, New York, 1981, pp. 304-307.

8. C.M. Wolfe, N. Holonyak Jr., and G.E. Stillman, Physical Properties of Semiconductors, Prentice Hall, Englewook Cliffs, New Jersey, 1989, pg. 318.

9. P.M. Stella and R.M. Kurland, “Thin Film GaAs for Space -- Moving out of the Laboratory”, Proceedings of the 23rd IEEE Photovoltaic Specialists Conference, (1993).

10. H.J. Hovel, Solar Cells, Chapter 7, Academic Press, (1975).

11. M.E. Nell and A.M. Barnett, “The Spectral p-n Junction Model for Tandem Solar Cell Design”, IEEE Transactions on Industrial Electronics, Volume ED-34, No. 2, May 1982.

12. L.C. Olsen, G. Dunham, F.W. Addis, D. Huber, and D. Daling, “Electro-optical Characterization of GaAs Solar Cells, Proc. 19th IEEE Photovoltaic Specialists Conference, (1987).

13. P.D. DeMoulin, C.S. Kyuno, M.S. Lundstrom, and M.R. Melloch, “Dark IV Characterization of GaAs p/n Heteroface Cells, Proc. 19th IEEE Photovoltaic Specialists Conference, (1987).

14. S.A. Ringel, A. Rohatgi, and S.P, Tobin, “An Approach Toward 25% Efficient GaAs Heteroface Solar Cells, IEEE Transactions on Electron Devices, vol. 36, No. 7, July 1989.

DISTRIBUTION LIST

AUL/LSE Bldg 1405 - 600 Chennault Circle Maxwell AFB, AL 36112-6424	1 cy
DTIC/OCP 8725 John J. Kingman Rd Ste 944 FT Belvoir, VA 22060-6218	2 cys
AFSAA/SAI 1580 Air Force Pentagon Washington, DC 20330-1580	1 cy
PL/SUL Kirtland AFB, NM 87117-5776	2 cys
PL/HO Kirtland AFB, NM 87117-5776	1 cy
Official Record Copy	
PL/VTP/Lt Keener Kirtland AFB, NM 87117-5776	2 cys
Dr. R. V. Wick PL/VT Kirtland, AFB, NM 87117-5776	1 cy